Manuscript Details

Manuscript number GEOT_2020_138

Title Step-over fault zones controlling geothermal fluid-flow and traver-tine formation (Denizli Basin, Turkey)

Abstract

In the Honalilar area (Denizli Basin, Turkey), the occurrence of banded Ca-carbonate veins and travertine deposits, represented by a dismantled fissure ridge-type depositional system, are the evidence of a Middle-Late Pleistocene exhumed, shallow, hydrothermal system. Their occurrence offers the best opportunity to: (i) reconstruct the fluid paths from the underground to the pal-aeo-surface, and (ii) analyse the role of fault zones in controlling the permeability and fluids cir-culation. Permeability developed in overstepping regional scale normal faults, with a slight left-lateral oblique-slip component. At the surface, faults favored the localization and development of a fissure ridge-type travertine deposit. At depth, the root of the hydrothermal system con-sists of W-E oriented fractures filled of up to 6.5 m thick Ca-carbonate veins, developed in a high dilatation zone. It corresponds to the step-over determined by the oblique-slip kinematics of the NW-striking main faults. The high dilatation step-over zone contrasted the progressive sealing induced by the concomitant Ca-carbonate deposition within the fractures, thus favoring permeability maintenance and fluids circulation for at least 200 ka. This evidence adds key inputs for predicting permeable volumes during geothermal exploration in areas affected by exten-sional tectonics. The main NW-oriented faults remained active even after the hydrothermal fluid flow, causing the dismantlement and progressive exhumation of the upper part of the hydro-thermal system.

Submission Files Included in this PDF

File Name [File Type]

Honalilar TEXT.docx [Manuscript File]

Fig. 1 - Carta generale.jpg [Figure]

Fig. 2 - Carta bordo Bacino Denizli.jpg [Figure]

Fig. 3 - Foto cava e scanline.jpg [Figure]

Fig. 4 - Zona di faglia.jpg [Figure]

Fig. 5 - Faglie ed indicatori cinematici e aspetto faglie.jpg [Figure]

Fig. 6 - Carta Geologica Golemezli.jpg [Figure]

Fig. 7 - Stereonet e impianto faglie.jpg [Figure]

Fig. 8 - Stress.jpg [Figure]

Fig. 9 - Relazioni cinematiche.jpg [Figure]

Fig. 10 - Travertino.jpg [Figure]

Fig. 11 - Vene bandate in generale.jpg [Figure]

Fig. 12 - Scanline.jpg [Figure]

Fig. 13 - relazioni di crossctutting.jpg [Figure]

Fig. 14 . per scanline1.jpg [Figure]

Fig. 15 - per scanline.jpg [Figure]

Fig. 16 - Indicatori cinematici.jpg [Figure]

Fig. 17 - diagramma relay.jpg [Figure]

Fig. 18 - modello finale.jpg [Figure]

Fig. 19 - Modello concettuale fissure ridge.jpg [Figure]

Step-over fault zones controlling geothermal fluid-flow and travertine formation (Denizli Basin, Turkey)

Andrea Brogi[a,b*], Mehmet Cihat Alçiçek[c], Domenico Liotta[a,b], Enrico Capezzuoli[d], Martina Zucchi[a], Paola Francesca Matera[a]

[a] University of Bari, Department of Earth and Geoenvironmental Sciences, 70125, Bari, Italy.
[b] CNR-IGG Pisa, Institute of Geosciences and Earth Resources, 56124, Pisa, Italy.
[c] University of Pamukkale, Department of Geology, 20070, Denizli, Turkey.
[d] University of Florence, Department of Earth Sciences, 50121, Florence, Italy.

[*] Corresponding author: andrea.brogi@uniba.it

Abstract
In the Honalilar area (Denizli Basin, Turkey), the occurrence of banded Ca-carbonate veins and travertine deposits, represented by a dismantled fissure ridge-type depositional system, are the evidence of a Middle-Late Pleistocene exhumed, shallow, hydrothermal system. Their occurrence offers the best opportunity to: (i) reconstruct the fluid paths from the underground to the palaeo-surface, and (ii) analyse the role of fault zones in controlling the permeability and fluids circulation. Permeability developed in overstepping regional scale normal faults, with a slight left-lateral oblique-slip component. At the surface, faults favored the localization and development of a fissure ridge-type travertine deposit. At depth, the root of the hydrothermal system consists of W-E oriented fractures filled of up to 6.5 m thick Ca-carbonate veins, developed in a high dilatation zone. It corresponds to the step-over determined by the oblique-slip kinematics of the NW-striking main faults. The high dilatation step-over zone hindered the progressive sealing induced by the concomitant Ca-carbonate deposition within the fractures, thus favoring permeability maintenance and fluids circulation for at least 200 ka. This evidence adds key inputs for predicting permeable volumes during geothermal exploration in areas affected by extensional tectonics. The main NW-oriented faults remained active even after the hydrothermal fluid flow, causing the dismantlement and progressive exhumation of the upper part of the hydrothermal system.

Key words
Geothermal systems, extensional tectonics, relay zones, banded Ca-carbonate veins, travertine, western Anatolia

1. Introduction
In scarcely permeable rock volumes, migration of geothermal fluids is strictly controlled by fault damage zones (Caine et al., 1996; Barbier, 2002; Rowland and Sibson, 2004; Zucchi, 2020) where fracture-array (Caine et al., 1996; Cox et al., 2001; Liotta et al., 2018) is consequence of fault kinematics (Sibson, 2000; Kim et al., 2003; Brogi, 2011a). Laboratory experiments, numerical simulations and fieldwork analyses demonstrated that the permeability of the fault damaged rocks is enhanced by orders of magnitude with respect to the host rock (i.e. protolith, in: Bruhn et al., 1990; Sibson, 1996; Evans et al., 1997; Caine and Forster, 1999; Jourde et al., 2002). Nevertheless, permeability of fault zones is not homogeneously distributed (Stober and Bucher, 2007; Zucchi et al., 2017) and, in addition, it changes through time during fault evolution (Sibson, 1987; Cox, 1999; Rowland and Sibson, 2004; Uysal et al., 2009; Bense et al., 2013) with modifications in the fault zone

architecture (Fyfe, 1987; Hancock et al., 1999; Polak et al., 2003; Uysal et al., 2009; Alt-Epping et al., 2013). Moreover, if saline fluids are permeating fractures, mineralization can develop (Bons et al., 2012) providing reduction of permeability. This latter effect is contrasted by new tectonic pulses, reopening previously sealed fractures (Curewitz and Karson, 1997; Uysal et al. 2007; Liotta et al., 2010). Consequently, permeability of a fault zone is extremely variable through time, and difficult to be predicted.

Permeability is considerably enhanced if two (or more) fault segments are interacting, as it is the case of the linkage zones and faults intersection areas (Curewitz and Carson, 1997; Brogi, 2004; Camanni et al., 2019; Liotta and Brogi, 2020). Interaction of fault segments generate multiple, commonly overlapping, minor structures, increasing the fracture density in limited rock volumes, where consequently, permeability is enhanced, from depth to surface (Curewitz and Carson, 1997; Hancock et al., 1999; Brogi et al., 2016a; Olvera-García et al., 2020). In this framework, step-over zones (or relay ramps) in normal fault settings are considered as among the most favorable structural conditions (Fossen and Rotevatn, 2016) to host geothermal fluid flow (James et al., 2011). For this reason, fault zones are considered of strategic interest for geothermal exploration. Furthermore, the knowledge of faults geometry, their timing and kinematics, as well as the understanding of the relationships between geological structures and fluid flow, are crucial for reducing the mining risk and for a responsible use of the geothermal resources. However, since exploration targets are at depth, information obtained by the study of exhumed geothermal systems represents the key to investigate the process linking permeability and fracture development.

Areas with travertine deposits (Ford and Pedley, 1996; Pentecost, 2005) offer the best opportunity to analyse how the deformation associated to a fault zone impacts on fluid circulation, favoring geothermal fluid migration from the deep reservoir up to the surface. Travertine (sensu Capezzuoli et al., 2014) is a terrestrial carbonate, formed from thermal springs discharging mainly Ca^{2+} and HCO_3^- saline fluids deriving from the interaction between fluids and deep, highly fractured, carbonate bodies (Brogi et al., 2016a and references therein). Basically, travertine deposits are considered indicators of tectonic activity (Hancock et al., 1999) and their analyses can contribute to define geometry, age and kinematics of the structures to which travertine deposits are associated (Altunel and Hancock, 1993a, 1993b; Çakır, 1999; Martinez-Diaz and Hernandez-Enrile, 2001; Brogi, 2004; Mesci et al., 2008; Brogi and Capezzuoli, 2009; Temiz and Eikenberg, 2011). Travertine are also suitable for accurate dating analyses through ^{14}C and $^{230}Th/^{238}U$ methods (Martinez-Diaz and Hernandez-Enrile, 2001, Altunel and Karabacak, 2005; Piper et al., 2007; Mesci et al., 2008; Temiz and Eikenberg, 2011; Nishikawa et al., 2012), thus permitting to date faults activity (cf. Muir-Wood, 1993; Çakır, 1999; Altunel and Karabacak, 2005; Uysal et al., 2007; Brogi et al., 2010; 2017; 2020).

When exhumation determined the exposition of the root of an hydrothermal system, the effects of the interplay between fractures and fluids circulation are measurable by studying the evolution of banded Ca-carbonate veins (banded travertine, in: Altunel and Hancock, 1993a, 1993b), representing the main mineralization in the fractures defining the fault zone. Chemical-physical variations of fluids properties (e.g., pressure, temperature and/or pH) trigger the filling fractures Ca-carbonate deposition (Uysal et al., 2009). Renewed tectonic activity can (re-)open the veins, therefore restoring the fluids circulation from which the growth of banded veins restart (crack-and-seal mechanism, Sibson, 1977, Ramsay, 1980). It follows that analysing banded Ca-carbonate veins in exhumed geothermal systems provides important inputs for understanding how fluids circulate within fault zones.

In this paper we describe the geometry of a well-exposed, Middle-Late Pleistocene exhumed geothermal system, from its palaeo-surface down to 100 m, i.e. from the dismantled travertine deposits to their feeding conduits, represented by banded Ca-carbonate veins.

This exhumed system is located in the northeastern part of the Denizli Basin (western Anatolia, Fig. 1) and consists of a “christmas tree-like” carbonate volume (about 25000 m^2 in plain view and 100 m in section), concentrated in a system of permeable damage fault zones where geothermal fluids were channeled. The peculiarity of this system is that fluid circulation was controlled by fractures of which width is up to 6.5 m, as determined by repeated crack-and-seal events. At the same time, these veins developed in a confined area where normal faults of regional relevance overlapped. Fluids reaching the surface formed a fissure ridge-type travertine deposit, progressively deformed during faulting, hence confirming the syn-tectonic travertine deposition.

We interpret the study area as a step-over zone between fault segments, developed in an extensional setting. Our results describe how such a zone represents a favorable volume to channel geothermal fluids toward the surface, giving inputs for geothermal exploration.

2. Geological outline

After the Alpine collisional stage, western Anatolia has been affecting by extensional tectonics since Neogene (Şengör & Yılmaz 1981). Extensional tectonics resulted in early-middle Miocene low-angle normal faults, determining core complex structures and supra-detachment basins~~, and subsequent~~ late Miocene-Present faults~~,~~ cross-cut~~ting~~ all the previous structures and ~~defining an interplay~~ of transfer and normal faults (Alçiçek et al., 2013) and related tectonic depressions, where continental sedimentation took place (e.g., Şengör and Yılmaz, 1981; Bozkurt, 2003; ten Veen et al., 2009; Alçiçek et al., 2013).
The Denizli Basin (Fig.1) is 50 km wide and 70 km long and is delimited by NW- and SE-~~trending~~ faults, developing since late Miocene and ~~accommodating about~~ 1300 m of continental sediments~~, at least~~ (Şimşek, 1984; Sun, 1990; Konak and Şenel, 2002; Konak, 2002; Koçyiğit, 2005; Kaymakçı, 2006; Alçiçek et al., 2007). The pre-Neogene bedrock consists of: (i) pre-Oligocene metamorphic rocks belonging to the Menderes Massif, and (ii) phyllite, metacarbonate and ophiolite-bearing carbonate-terrigenous succession of the Lycian Nappes. The Menderes Massif is the structurally deepest outcropping unit; it is formed by HP–LT marble, quartzite and garnet-bearing micaschist hosting Palaeozoic-Cenozoic granitoids (Pamir and Erentöz, 1974; Şengör and Yılmaz, 1981; Okay, 1989; Sun, 1990; Bozkurt, 2001; ten Veen et al., 2009; van Hinsbergen, 2010; van Hinsbergen and Schmid, 2012). This unit is tectonically overlain by the Lycian Nappes (Collins and Robertson, 1997), through a regional extensional detachment as described in the surrounding~~s~~ areas (Okay, 1989; Sun, 1990; Gündo☒an et al., 2008; ten Veen et al. 2009, van Hinsbergen et al. 2010). Extension ~~is~~ accompanied by magmatism and ~~hydrothermalism~~, as ~~it is testified~~ by the diffuse hydrothermal mineralization and travertine deposits characterising western Anatolia (Ozkul et al., 2013; Brogi et al., 2016b).
The Neogene and Quaternary Denizli Basin succession, referred to as the Denizli Group, is subdivided into four lithostratigraphic units and consists of alluvial-fan, fluvial, and lacustrine deposits (Şimşek, 1984). From early Miocene, the Denizli Basin was controlled by the fault system ~~located to~~ its SW ~~part whereas, from~~ early Quaternary~~, such a Basin~~ enlarged due to the activation of the NE fault system referred to as the Pamukkale, Akköy and Tripolis fault segments (Altunel and Hancock, 1993a,b; Altunel, 1994; Hancock et al., 1999; Alçiçek et al., 2007; Brogi et al., 2014~~a~~). These ~~latter~~ controlled the location of the major travertine/tufa deposits (Ozkul et al., 2013; Capezzuoli et al., 2018; Alçiçek et al., 2019), presently characterising this sector of the Basin (Fig. 1).
The Gölemezli travertine (Çakır, 1999) was described as an isolated deposit consisting of two fissure ridges (around 100 m long) developed in a relay ramp connecting two fault segments named as the Tripolis and Akköy faults (Fig. 2). The volume of travertine deposit, about ~35 m thick over an area of <1 km^2, is estimated to be ~0.035 km^3 (Sun, 1990; Alçiçek et al., 2018). The deposit ~~result~~ dominantly ~~formed by~~ multigenerational and multicoloured Ca-carbonate veins (Özkul et al., 2013; Capezzuoli et al., 2018). These developed along vertical/subvertical fault zones and extensional fissures affecting both the metamorphic substrate and the overlying bedded travertine. The age of the Ca-carbonate veins is ~~encompassed~~ between 504.232 ±72.608 and 310.677± 5.764 ka (Capezzuoli et al., 2018).

2.1 The Pamukkale fault system

The northeastern shoulder of the Denizli Basin is ~~delimited~~ by NW-striking, SW-dipping, normal faults affecting the Neogene–Quaternary continental sediments (Fig. 2), juxtaposing these sediments ~~to~~ the Palaeozoic and Mesozoic metamorphic units (Menderes Units and Lycian Nappe) (Şaro☒lu et al., 1987, 1992; Çakır, 1999; Hancock et al., 1999; Koçyi☒it, 2005; Kaymakçı, 2006; Alcicek et al., 2007). This normal fault system cuts, and is crosscut, by almost orthogonal faults (NE-striking) interpreted as transfer faults active during extensional tectonics (Kaymakçı, 2006; Brogi et al. 2014; 2016b; Alcicek et al., 2018).
Activity of such a fault system is ~~encompassed~~ between early Miocene and Holocene, on the basis of the age of the sediments involved in the deformation and on the relationships between faulting and travertine deposition (Altunel and Karabacak, 2005; Brogi et al., 2016b; Capezzuoli et al., 2018). Present deformation is

indicated by: i) the location of ~~the~~ historical and recent earthquakes (Utku, 2009; Irmak, 2013); ii) the alignments of active geothermal manifestations; iii) the on-going deposition of travertine (Lebatard et al., 2014; Boulbes et al., 2014).

Kinematic data on the NW-striking fault segments indicate a main normal dip-slip component during Quaternary (Altunel and Hancock, 1993a; Çakir, 1999). This is also supported by the offset of the Roman artefacts along the fault segment ~~passing~~ through Hierapolis archaeological site (Altunel and Hancock, 1996; Piccardi, 2007). Nevertheless, a left-lateral strike- to oblique-slip kinematics characterises the older fault activity as indicated by Altunel and Hancock (1993a) and Çakir (1999).

A different kinematic~~s~~ characterises the NE-striking faults, on which right- and left-lateral oblique-slip movements superimposed the older normal ~~ones~~ (Kaymakci, 2006; Brogi et al., 2014; Brogi et al., 2016b; Van Noten et al., 2013).

However, both the NW- and NE-striking fault systems~~,~~ played a fundamental role for the overall hydrothermal circulation and fluid upwelling (Alçiçek et al., 2013). Thermal springs (up to 57 °C, Bülbül, 2000; Bülbül et al., 2005; Alçiçek et al., 2016) and travertine deposits (Altunel and Hancock, 1993a, b, c; Altunel, 1994) are aligned along the main fault segments, thus indicating a close relation between these structures and fluid pathways. Furthermore, the hydrothermal circulation is mainly concentrated in those areas near~~by~~ the intersection between the NE- and NW-~~trending~~ faults, where the rock volumes are ~~deeply damaged~~.

In this context, the syn-tectonic fissure ridge-type travertine deposits (Bargar, 1978) are developing along the traces of both NE- and NW-trending structures belonging to the Pamukkale system. As examples, the NW-trending Çukurbag and Kamara fissure ridges have been described in details by several authors (De Filippis et al., 2012 with references therein; Brogi et al., 2014, Brogi et al. 2016b), being key morpho-tectonic features and showing clear syn-tectonic hydrothermal fluid flow with the related travertine deposition (Altunel and Hancock, 1993a, 1996; Altunel, 1994; Hancock et al., 1999). The hydrothermal circulation along fault zones ~~is however occurring~~ since Pleistocene, as testified by the mineralised, partly exhumed, damaged rock volumes associated ~~to~~ NE- and NW-~~trending~~ fault zones. Mineralization consists of centimeter to meter thick syn-tectonic banded Ca-carbonate veins with minor content of Fe-hydroxides. These Middle Pleistocene to Holocene veins (Altunel and Karabacak, 2005; Özkul et al., 2013, De Filippis et al., 2012; Brogi et al., 2016b) crosscut the metamorphic rocks of the Menderes Massif and the Neogene sedimentary layers. The Ca-carbonate veins include cm-to-dm thick fragments of the host rocks, although altered by hydrothermal circulation and cemented by calcite. In particular, up to meters-sized Ca-carbonate veins can occasionally develop parallel to bedding and/or schistosity surfaces. Independent~~ly~~ of their attitude and thickness, Ca-carbonate veins are always filled ~~of~~ banded onyx-like fibrous calcite/aragonite crystals, with symmetric, mm-thick laminae of different colors (reddish, yellowish, whitish and grey- greenish) formed during repeated crack-and-seal episodes (Uysal et al., 2007).

3. Data analysis

Field mapping and structural analyses were carried out along a tract of the northeastern margin of the Denizli Basin, in the Honalilar area, in the ~~surrounding~~ of the travertine exposure and within the quarry, where travertine deposits and Ca-carbonate veins were exploited (Figs 2 and 3). The morphological scarp and quarry location permitted us to collect data from the paleo-surface, now at top-hill, to ~~the deep~~ part of the hydrothermal system, now at the base of the scarp, for a total exposed height of about 100 m. Outcrop conditions were optimal in the quarry (where the saw-cuts exposed about 100 m of travertine and feeder conduits). ~~Differently~~, due to alteration and vegetation only ~~spotted~~ outcrops were visible at the base of the hill, along its flanks, and at ~~top-hill~~ (Fig. 3).

In the following, for sake of clarity, the presentation of data is separated in two different sections address~~ed~~ to the description of the fault system and its impact on the travertine and Ca-carbonate veins deposition.

3.1 The faults system in the Honalilar area

The Honalilar area is located along the Pamukkale fault system, ~~delimiting~~ the Denizli Basin to the NE (Fig. 2). In this area the faults ~~lose their lateral continuity~~ to form a step ~~just~~ centered in the area where travertine deposits and associated banded Ca-carbonate veins are located (Fig. 3).

The slip surfaces of the major faults are not exposed, although ~~forming~~ well pronounced morphological slope, (Fig. 3). These faults juxtapose the metamorphic rocks (marble, quartzite and micaschist) of the Menderes Unit with the Neogene terrigenous and carbonate successions filling the Denizli Basin (fault segment 3, in: Figs 2 and 3). Nevertheless, minor faults (including fault segment 2 in: Figs 2 and 3) and fractures are exposed in the footwall damage zone of the main faults (Fig. 4). The bulk of the minor faults is characterized by vertical offsets of few meters and by core zones ranging from 0.5 to 10 cm. Their damage zones can reach up to 10 m. These faults exhibit kinematic indicators, consisting of slickenlines with steps (Fig. 5) or, in some cases, calcite/quartz fiber-steps and chatter marks.

Kinematic data have been collected in 16 structural stations distributed along the main fault segments and in the step-over zone (Fig. 6), nearby the quarry area.

Outside the step-over zone, the two interacting NW-SE striking fault zones (eastern and western fault zones, Fig. 7 and 8) are instead characterised by a slight left-lateral oblique-slip kinematics, with pitches ranging from 65° to 84° with an average pitch of about 75°. ~~It~~ implies a 0.26 average ratio between the ~~vertical and horizontal off-set~~ components (Fig. 9a). ~~The horizontal component gave rise to the high dilation component~~ within the step-over zone (Fig. 9b-c) ~~and favored the the normal kinematics of the faults (Fig. 8)~~, which was also induced by the ~~vertical component of the~~ fault segments 1 and 3.

3.2 The ~~epigean and hypogean~~ travertine depositional system

This is described in two parts: the first is about the ~~epigean~~ (~~upper~~) part, characterized by bedded travertine deposits (i.e., Ca-carbonate deposition occurred at the ground-air boundary), also described in Capezzuoli et al. (2018); the second part ~~is addressed to describe the hypogean~~ part (the upper root of the hydrothermal system), defined by the feeder conduits, now highlighted by banded Ca-carbonate veins grown within the damage zones of the main faults~~,~~ and in lateral pre-existing discontinuities.

The epig~~ean~~ part

Travertine deposits, up to 15 m thick, are formed by bedded/laminated ~~continental~~ limestone. These deposits were dissected by normal faults and are now exposed (i) at the top of the hill (ca. 520 m a.s.l.) in the footwall of the faults system, (ii) on the fault hanging wall, overlying unconformably Neogene sediments and (iii) on the slope, in the fault zone (Figs 3 and 6).

At the top of the hill, a partly dismantled travertine fissure ridge-type deposit, up to 50 m long, ~~NW-SE trending,~~ has been reconstructed. Such a morpho-structural element overlies a matrix-supported polygenic breccia, directly resting on the metamorphic units (Fig. 10a-b), locally containing rounded cobbles and pebbles that progressively passed to microbial carbonate laminites and abiotic crystalline crusts (Fig. 10c-e). The microbial laminites, typical of low-energy environment, consist of subparallel sets, up to 20 cm thick, of porous crust made up of spongy bindstone mats with peloidal fabric. Many pores show an elongated oblong shape, which can be ascribed to gas-escaped bubbles entrapped, or bound, by microbial mats. Blocky sparite cement is locally present with equant crystals sized 150–300 μm. Microbial laminae in places encrust the components of the basal breccia, although, in some cases such laminae ~~are~~ alternate~~d~~ with (or pass laterally to) crystalline crusts. The crystalline crusts, generated by laminar flux along medium to steep slopes are made up of 1–10 cm thick, linear to curvilinear, calcite laminae formed of rows of densely crowded feather-like/ dendritic crystals (Fig. 10).

These beds, made up of crystalline crusts and microbial laminites, are tens of centimeters thick in average, and show variable primary dipping attitudes (from almost vertical to sub-horizontal), although, on the whole, dipping away from the NW-SE oriented axial zone.

NW-SE striking sub-vertical banded calcite veins, up to 90 cm thick (Fig. 10c), crosscut the bedded travertine in the slopes of the fissure ridge. The fissure ridge occurrence, as well as its orientation (Fig. 6), indicate the distribution of structurally controlled palaeo-thermal springs from which the travertine deposit ~~took place~~. ~~Such~~ fissure ridge represents the proximal part of this depositional system, while its distal part is partially exposed in the slope and hanging wall of the fault system. In these sectors, travertine is strongly deformed by E-W striking faults and cut by numerous cm- to dm-thick, NW-SE and E-W oriented banded calcite veins. Travertine consists of sub-horizontal or gently inclined (5°-10°) cm-to-m thick beds of microbialite (laminite and lime-mudstone/peloidal micrite facies). Meter-thick layers of well-bedded crystalline crusts show lateral correlation with microbial lithofacies. Lime mudstone occurs in planar to wavy layers up to 4 m thick (on average 20–30 cm), of a grey, dense homogeneous micritic/ microsparitic, ~~sometimes~~ slightly argillaceous carbonate made up of unfossiliferous, clotted/peloidal and/or structureless micrite (Fig. 10d-e). The layers locally alternate with, or laterally pass to, crystalline crusts and microbialites. Such facies association ~~deposited~~ in low-energy flat/wetland settings (palustrine, distal pools), corresponding to the bottom of slope terraces and/or shallow lakes.

The ~~hypogean~~ part

This is visible, in vertical sections, from the palaeosurface down to about 100 m due to the saw-cuts of the quarry. It consists of a network of onyx-like crystalline veins (banded Ca-carbonate veins) ~~crossing~~ the metamorphic rocks and isolating cm- to m-thick volumes of brecciated host~~ing~~ rocks (Fig. 11). These veins ~~coincide~~ with the feeder conduits that channeled the hydrothermal fluids up to the surface, where travertine deposited (Fig. 10). The Ca-carbonate veins veins are concentrated in an area of about 400 x 600 m (quarry area) and are only ~~occasionally~~ present outside. In the quarried area, veins are thicker (up to 6 m, Fig. 12a-c)~~,~~ and closely spaced: up to 8 veins per 10 m (Fig. 12d). Their concentration and overall size rapidly decreases from the quarry area ~~toward the surroundings~~, while veins pinch out west- and eastwards in a short distance (Fig. 6).

The Ca-carbonate veins are W-E ~~trending~~ and steeply dipping toward S - SW (Fig. 12e). In some places these are locally sheared with a normal movement, as affected by faulting during and after their development (Fig. 12f). The vein~~s~~ texture is characterized by mm-to-cm thick, parallel and/or subparallel vertical bands of different colors: white, light-transparent and more rarely brownish bands (Fig. 13a).

The contact between veins and host rock is sharp; ~~occasionally~~, centimeter-scale breccia fragments of Ca-carbonate veins veins are embedded in the same vein (intraclastic breccia), thus suggesting continuous deformation through time (Fig, 13a). Furthermore, the same microcrystalline coat locally encrusts/cements the clasts of small lenses (up to 1.50 m) of extraclastic breccia derived from the metamorphic (Menderes Massif) and Neogene substrate (Fig. 13b): this indicates an enlargement of the deformation volume and the syn-tectonic development of calcite veins that, in some cases, show internal cross-cutting relationships (from sinuous to orthogonal; Fig. 13c), suggesting repeated crack-and-seal events.

Vein crystals grew normal to the wall-rock toward the central part of fractures, thus forming symmetrical, isopachous or, less frequently, botryoidal mm-to-cm thick crusts (Fig. 13b). Banded veins are commonly completely sealed, although discontinuous voids rimmed by festoons can locally be observed in the central part of the vein, where their suture occurs.

Scan lines have been measured in order to reconstruct veins distribution and their geometrical setting in the whole quarry (Fig. 3). Scan lines, ~~settled~~ orthogonally to the veins, were subdivided in several segments to be adapted to the morphological setting and to the quarry cuts. By this, a total of 135 m was measured in detail (Fig. 12). The location of the scan lines does not correspond with their progressive numbering which, instead, followed the temporal criterion of acquisition.

Describing the scan lines starting from north (Fig. 12), scan line 1 is characterised by WNW-ESE ~~trending~~ cm- to dm-size banded veins, for about 15 m from its beginning. These veins are syntaxial and subvertical, crossing micaschist and quartzite of the Menderes Massif (Fig. 14a-b), and correspond to fault zones (Fig. 14a). From 40 to 58 m, the metamorphic rocks are cataclastic, displaying a quartzite and micaschist brecciated texture, with clasts cemented by yellowish carbonate and crossed by cm-size calcite veins (Fig. 14c-d). This cataclastic level is part of the damaged volume of the fault segment 1 ~~delimiting~~ the step-over zone (Fig. 3 and 12), of which slip surface is covered by the debris as indicated in Fig. 12a.

~~Differently~~, the next scan line (scan line 10) begins with a 70 cm thick W-E ~~trending~~ banded vein, followed by a 6 m thick breccia, made up of quartzite clasts, cemented by a yellowish calcite~~, mostly~~ (Fig. 15a-b). This breccia is locally crossed by W-E ~~trending~~, sub-vertical banded veins (Fig. 15c). At the end of the scan line, for at least 1.5 m, a thick banded vein occurs. This ~~latter has its extension in~~ the next scan line (scan line 9), passing through an at least 10 m thick, W-E ~~trending~~, sub-vertical vein, locally embedding lenses of up to 40 cm thick tectonic breccia (Fig. 12).

Scan line 8 displays a 6 m thick lithon of quartzite and micaschist. Such a lithon maintained almost intact its primary fabrics, although brecciated volumes characterise portions at the contact with the banded veins. A ~~c.~~ 80 cm thick vein ~~trends~~ W-E and steeply dips southwards. It passes to a 2.6 m thick breccia delimiting a cataclasite volume of metamorphic rock, embedded within the vein, ~~of which width is~~ 6 m, up to the end of scan line 8. The extension of such a vein is displayed in scan lines 7 and 6, where it ~~comprehends~~ 4 main lenses of a tectonic breccia cemented by yellowish carbonate and made up of quartzite and micaschist elements.

Scan line 2 begins with a micaschist lithon preserving its primary fabrics. It is followed by 1 m thick tectonic breccia and a very continuous banded Ca-carbonate vein~~s~~, detected for other 6 m~~eters~~. Such a vein characterises completely the scan line 3 (only 3 m long). Here, a 50 cm tectonic breccia lens is also recognized.

Scan line 5 starts with about 10 m thick breccia, made up of quartzite, locally cemented by yellowish calcite and crossed by a 40 cm thick Ca-carbonate veins vein. It follows about 3.5 m thick lithon, made up of quartzite and micaschist with their primary fabrics, although brecciated for about 3 m where a ~~c.~~ 80 cm thick banded vein affects the lithon.

In some cases, banded veins are crossed by slip surfaces with clear kinematic indicators. These faults dissect the veins producing localized cataclasite ~~levels~~. Kinematic indicators consist of mechanical striations and calcite fiber-steps, thus suggesting a fluid assisted faulting process (Fig. 16a-b). In other cases, the vein formation is accompanied by development of cm- to dm-thick extensional jogs (Fig. ~~16d~~). Banded Ca-carbonate veins veins and faults have a common W-E orientation (Fig. 12e-f).

Outside the quarry yard, outcrops are discontinuous and it was no longer possible to take measurements by scan lines. Nevertheless, a fault zone injected by cm- to m-thick banded calcite veins juxtapose the travertine deposits ~~to~~ the metamorphic rocks. ~~Travertine results~~ strongly fractured, and each fracture is filled by banded Ca-carbonate veins. In some cases, banded veins form a network with mainly sub-vertical and sub-horizontal veins, ~~these~~ latter following the travertine beds.

The kinematic indicators collected in the step-over zone indicate W-E striking faults with a dominant normal component (Figs 8 and 12) and, in part, dissecting the W-E oriented banded veins. These ~~latter developed~~ within the fault zones, therefore suggesting a continuous faulting activity assisted by hydrothermal fluid~~s~~ circulation during earlier stages.

The different kinematics between faults hosting the banded veins in the quarry area and the eastern/western faults (i.e. fault segments 1 and 2, Fig. 7) is framed in the step-over zone setting as discussed in the next paragraph.

4. Discussion

The Honalilar area was first~~ly~~ investigated by Çakir (1999) who considered the banded Ca-carbonate veins as travertine deposits associated ~~to~~ faults. At the top of the hill, this author documented two fissure ridges (about 100 m long) and slope-facies travertine deposits. In the same area, we recognised only one fissure ridge, partly dismantled (Fig. 10c), and a parallel banded Ca-carbonate vein cutting the travertine deposit (Fig. 6), which probably corresponds to the second fissure ridge reported by Çakir (1999). Contrarily, Özkul et al. (2013) described multicolored Ca-carbonate veins crossing the metamorphic substratum and bedded travertine deposits. According to Özkul et al. (2013), travertine deposits are exposed at the top of the hill and in the southern part of the quarry, where travertine deposits were offset by NW-SE and W-E striking faults (Fig. 6).

~~Although~~ the broad exposures ~~favored~~ by the quarry cuts, the transition and relationships between the banded Ca-carbonate veins and the bedded travertine is not visible (i.e., how the carbonate deposition changed from depth to ground-air boundary). Nevertheless, their link is clear as also documented by Capezzuoli et al. (2018). We therefore assume that the described Ca-carbonate veins developed within fractures that channeled fluids to the surface, where the related fault-controlled travertine deposits (i.e. fissure ridges) were located. These ~~latter~~ are today eroded and dismantled due to erosion and progressive faulting.

~~Noteworthy~~, banded Ca-carbonate veins and travertine deposits occur only in a restricted area of about 400 x 600 m, delimited by two main NW-SE striking fault segments~~, SW-dipping~~ (Fig. 6) ~~and forming~~ a fault step-over zone (Peacock and Sanderson, 1991, 1994; Childs et al., 1995). This ~~accounts~~ for a close relationship between ~~such deformational~~ zone and circulation of Ca-enriched geothermal fluids.

The main faults defining the step-over zone are characterised by a dominant normal component (Figs 7 and 8). Nevertheless, the banded veins show a different orientation with respect to the fault segments ~~delimiting~~ the step-over zone~~: they form angles ranging from~~ 34° to 52° (Fig. 6). On the other hand, overstepping zones are characterised by fault/fracture segments with a geometrical pattern resulting from the local stress (Sibson 1985, 1996), where tensile and shear failure independently and locally developed to link fault segments with different orientation and kinematics (Childs et al., 1995; Camanni et al., 2019). The unusual thickness of the banded Ca-carbonate veins (Fig. 11) accounts for an important dilatational component affecting the step-over rock-volume. This feature, coupled with their angular relation with the main faults, accounts for a strike-slip component of the faults parallel to the basin, accommodated by the step-over zone (i.e. releasing step over zone, in: Kim et al., 2004 and references therein). It implies two left-lateral strike-slip faults bounding the area, as ~~it was already~~ hypothesised by Çakir (1999) for the study area. Nevertheless, our kinematic data indicate a different scenario: the main faults show a dominant normal ~~kinematics~~ with a very minor left-lateral component (Fig. 7). This kinematic setting account for a relay zone linking normal faults instead of strike-slip faults. In this view, the fault length - relay width ratio is fitting with several step-over zones in extensional settings, as documented around the world (Fig. 17).

In addition, according to Mayolle et al. (2019) and Childs et al. (2019), fractures linking normal fault segments are not purely dilatational in extensional settings, as it is the case of the Honaliar area. This apparent incongruence could be explained by analysing the configuration of the step-over zone that is not deriving from adjacent parallel and en-echelon fault segments, as described for most cases by several authors (Larsen, 1988; Peacock and Sanderson, 1991, 1994; Childs et al., 1995; Cartwright et al., 1996; Crider and Pollard, 1998; Brogi, 2011; Peacock, 2002; Fossen and Rotevatn, 2016; Nixon et al., 2018). In our case, the overlapping faults (fault segments 1 and 3, Figs 3 and 7) diverge just ~~in correspondence of~~ the overlapping zone: in fact, the south-eastern fault segment (fault segment 1, named Pamukkale ~~F~~ault by Çakir, 1999) abruptly changes its strike, passing from N130° to about N160° (Fig. 7). This configuration excludes a pure strike-slip dilatation step-over zone linking fault segments with an en-echelon configuration and accounts for a step-over zone linking two diverging fault~~s~~ segments, with a dominant normal component (pitches ranging from 65° to 80°, 75° on average). This setting ~~guaranties~~ dilatation and consequent high permeability. This ~~adds new inputs~~ for predicting targets during geothermal exploration in extensional settings. Fluid paths are, in fact, controlled by the orientation of the intermediate stress axis (Sibson 2000): closer to the vertical, easier to channel deep fluids, increasing the hydraulic conductivity. It derives that at least ~~an oblique kinematics is~~ crucial to easily channel geothermal fluids from depth to the surface. At the same time, the high dilatation within the step over zone ~~contrasts~~ the sealing process deriving ~~by~~ the progressive Ca-carbonate deposition from the geothermal fluids, related to the CO_2 degassing (Mancini et al., 2019). At the surface, the effect of the CO_2 degassing from structurally controlled thermal springs consists of sinter deposits: travertine (i.e. carbonate sinter deposit) is the most widespread deposit forming nearby thermal springs, if the hydrothermal fluids have suited salinity (Pentecost, 1~~995~~). If this is the case, geothermal fluids are characterised by high sealing capacity when CO_2 degassing occurs. This process ~~contrasts~~ permeability in the bedrock, inhibiting fluids circulation although new fractures, induced by faulting, can reopen the existing conduits enhancing again fluid~~s~~ flow (Curewitz and Karson, 1997)~~,~~ during fault-valve behavior (cf. Sibson, 1981; Shelly et al. 2015; Ruhl et al., 2016). It follows that faulting and fluid~~s~~ flow are contemporaneous to travertine deposition and the Ca-carbonate mineralization within the fault zone becomes indicative of the age of the tectonic activity (Hancock et al. 1999) and hydrothermal circulation (Fouke et al., 2000; Simsek et al., 2000). In this case, we can refer the age of faults and the geothermal circulation to the time interval between about 504 and 310 ka (Capezzuoli et al. 2018) at least. In this view, during Middle Pleistocene, the step-over zone ~~developed~~ together with hydrothermal fluids flow, lasting for about 200 ka. It implies that the present hydrothermal circulation occurring in the Pamukkale area (Alçiçek et al., 2019 with refereces therein) could be controlled by ~~same~~ structural configurations, migrated through time toward the depocenter of the Denizli Basin, where active faults occur.

All these circumstances make the Honalilar exhumed hydrothermal system a site that offers the best conditions for ~~getting inputs to understand~~ the present geothermal circulation in the Denizli Basin and ~~all~~ areas around the world~~, showing~~ similar geological settings.

5. Conclusions

Combining data from ~~the mineralization occurred~~ in ~~the~~ fossil, exhumed hydrothermal system with structural and kinematic settings, we reconstructed the structural control ~~on the~~ about 200 ka long-living geothermal system, controlled by interacting faults in the extensional setting ~~characterizing~~ western Anatolia. Hydrothermal fluids rose up from a deep reservoir to surface~~,~~ through the damage ~~fault zones~~ developed in the step-over linking regional normal faults.

The structural and kinematic setting highlights a step-over zone, derived by the interaction of aligned faults, with dominant normal ~~component~~ and slight left-lateral movement (Fig. 18a). The master faults ~~configuration~~, coupled with their reconstructed kinematics, favored dilatational volumes within the step-over zone, where mode I and mode II fractures developed in response to the orientation of the regional and local stress field (Fig. 18b). Within the step over zone, the developing fractures and normal faults, steeply dipping toward south, formed in a high dilatation environment offering the best opportunity to generate permeability and circulation of large volumes of geothermal fluids. The crack-and-seal mechanism controlled fluid~~s~~ circulation within the fault zones and favored the formation of a widespread network of Ca-carbonate banded calcite veins, up to 6.5m thick, as result of the competition between extension and sealing process (Fig. 18c). At the surface, the Ca-carbonate banded veins should correspond to fissure ridge-type travertine deposits with a geometric configuration as illustrated in Fig. 19. It derives that Ca-carbonate banded veins and travertine deposits are primary features to be analysed for reconstructing the tectonic control on the geothermal fluid~~s~~ flow in ~~the~~ upper crustal levels. This result adds key inputs for predicting permeable volumes during geothermal exploration in areas affected by extensional tectonics.

Acknowledgments

Marco Meccheri, beloved friend and colleague, passed away in December 2016. Together with him, we started our study in the Honalilar quarry and surroundings. Marco deeply contributed in the reconstruction of the structural setting we are illustrating in this paper, which is dedicated to his memory. We have reported his thoughts, remembering his enthusiasm and huge passion for geology and Turkey. Marco is still in our minds, and his footprints are forever imprinted in the rocks exposed in this part of Anatolia.

This paper is the result of an international bilateral cooperation between TUBITAK (Scientific and Technological Research Council of Turkey) and CNR (National Research Council of Italy): grant number 113Y551. We are grateful to Mr. Barbaros Ozcelik for having permitted us to visit his quarry several times.

References

Alçiçek, H., Varol, B., Özkul, M., 2007. Sedimentary facies, depositional environments and palaeogeographic evolution of the Neogene Denizli Basin of SW Anatolia, Turkey. Sediment. Geol. 202, 596–637. https://doi.org/10.1016/j.sedgeo.2007.06.002

Alçiçek, M.C., Brogi, A., Capezzuoli, E., Liotta, D., Meccheri, M., 2013. Superimposed basins formation during the Neogene–Quaternary extensional tectonics in SW-Anatolia (Turkey): insights from the kinematics of the Dinar Fault Zone. Tectonophysics 608, 713–727. https://doi.org/10.1016/j.tecto.2013.08.008

Alçiçek, H., Bülbül, A., Alçiçek, M.C., 2016. Hydrogeochemistry of the thermal waters from the Yenice Geothermal Field (Denizli Basin, southwestern Turkey). J. Volcanol. Geoth. Res. 309, 118–138. http://dx.doi.org/10.1016/j.jvolgeores.2015.10.025.

Alçiçek, H., Bülbül, A., Brogi, A., Liotta, D., Ruggieri, G., Capezzuoli, E., Meccheri, M., Yavuzer, İ., Alçiçek, M.C., 2018. Origin, evolution and geothermometry of the thermal waters in the Gölemezli Geothermal Field, Denizli Basin (SW Anatolia, Turkey). J. Volcanol. Geoth. Res. 349, 1-30. https://doi.org/10.1016/j.jvolgeores.2017.07.021

Alçiçek, H., Bülbül, A. Yavuzer, İ., Alçiçek, M.C., 2019. Origin and evolution of the thermal waters from the Pamukkale Geothermal Field. J. Volcanol. Geoth. Res. 372, 48-70. https://doi.org/10.1016/j.jvolgeores.2018.09.011

Alt-Epping, P., Diamond, L.W., Häring, M.O., Ladner, F., Meier, D.B., 2013. Prediction of water–rock interaction and porosity evolution in a granitoid-hosted enhanced geothermal system, using constraints from the 5 km Basel-1 well. Applied Geochemistry, 38, 121-133. https://doi.org/10.1016/j.apgeochem.2013.09.006

Altunel, E., 1994. Active Tectonics and the evolution of Quaternary travertines at Pamukkale, Western Turkey. (PhD Thesis), University of Bristol (236 pp).

Altunel, E., Hancock P.L., 1993a. Active fissuring and faulting in Quaternary travertines at Pamukkale, western Turkey. Z Geomorph NF 94:285–302.

Altunel, E., Hancock, P.L., 1993b. Morphology and structural setting of Quaternary travertines at Pamukkale, Turkey. Geologic Journal 28:335– 346. https://doi:10.1002/gj.3350280312

Altunel, E., Hancock, P.L., 1993c. Pamukkale travertenleri kaç yaşında? Bilim ve Teknik Dergisi 26 (308), 496, 497

Altunel, E., Hancock, P.L., 1996. Structural attributes of travertine-filled extensional fissures in the Pamukkale Plateau, Western Turkey. Int. Geol. Rev. 38, 768–777. https://doi.org/10.1080/00206819709465360

Altunel, E., Karabacak, V., 2005. Determination of horizontal extension from fissure-ridge travertines: a case study from the Denizli Basin, southwestern Turkey. Geodin. Acta 18, 333–342. https://doi.org/10.3166/ga.18.333-342

Barbier, E., 2002. Geothermal energy and current status: An overview. Renewable and Sustainable Energy Reviews 6, 3–65. https://doi.org/10.1016/S1364-0321(02)00002-3

Bargar, K.E., 1978. Geology and thermal history of Mammoth Hot springs, Yellowstone National Park, Wyoming. United States Geological Survey Bulletin 1444, 1–55. https://doi.org/10.3133/b1444

Bense, V.F., Gleeson, T., Loveless, S.E., Bour, O., Scibek, J. 2013. Fault zone hydrogeology. Earth-Sci. Rev. 127, 171–192. https://doi.org/10.1016/j.earscirev.2013.09.008

Bons P.D., Elburg, M.A., Gomez-Rivas, E., 2012. A review of the formation of tectonic veins and their microstructures. J. Struct Geol, 43, 33-62. https://doi.org/10.1016/j.jsg.2012.07.005

Boulbes, N., Mayda, S., Titov, V.V., Alçiçek, M.C., 2014. Les grandsmammifères pléistocènes des travertins du Bassin de Denizli, Sud-ouest de l'Anatolie, Turquie. Anthropologie 118, 44–73. https://doi.org/10.1016/j.anthro.2014.01.001

Bozkurt, E., 2001. Neotectonics of Turkey – a synthesis. Geodin. Acta 14, 3-30. https://doi.org/10.1080/09853111.2001.11432432

Bozkurt, E., 2003. Origin of NE-trending basins in western Turkey. Geodin. Acta 16, 61-81. https://doi.org/10.1016/S0985-3111(03)00002-0

Bruhn, R.L., Yonkee, W.E., Parry, W.T., 1990. Structural and fluid-chemical properties of seismogenic normal faults. Tectonophysics 175, 139–157. https://doi.org/10.1016/0040-1951(90)90135-U

Brogi, A., 2004. Faults linkage, damage rocks and hydrothermal fluid circulation: tectonic interpretation of the Rapolano Terme travertines (southern Tuscany, Italy) in the context of the Northern Apennines Neogene-Quaternary extension. Eclogae Geol. Helv. 97, 307–320. DOI 10.1007/s00015-004-1134-5

Brogi, A., 2011a. Variation in fracture patterns in damage zones related to strike- slip faults interfering with pre-existing fractures in sandstone (Calcione area, southern Tuscany, Italy). J. Struct. Geol. 33, 644–661. https://doi.org/10.1016/j.jsg.2010.12.008

Brogi, A., 2011b. Bowl-shaped basin related to low-angle detachment during continental extension: the case of the controversial Neogene Siena Basin (central Italy, Northern Apennines). Tectonophysics 499, 131-148. https://doi.org/10.1016/j.tecto.2010.12.005

Brogi, A., Capezzuoli, E., 2009. Travertine deposition and faulting: the fault-related travertine fissure-ridge at Terme di S.Giovanni, Rapolano Terme (Italy). Int. J. Earth Sci. 98, 931–948. DOI 10.1007/s00531-007-0290-z

Brogi, A., Capezzuoli, E., Aqué, R., Branca, M., Voltaggio, M., 2010. Studying travertine for neotectonics investigations: Middle–Late Pleistocene syn- tectonic travertine de- position at Serre di Rapolano (Northern Apennines, Italy). Geol. Rundsch. 99, 1383–1398. DOI 10.1007/s00531-009-0456-y

Brogi, A., Capezzuoli, E., Alçiçek, M.C., Gandin, A., 2014. Evolution of a fault-controlled travertine fissure-ridge in the western Anatolia extensional province: the Çukurbag fissure-ridge (Pamukkale, Turkey). J. Geol. Soc. London 171, 425- 441. https://doi.org/10.1144/jgs2013-034

Brogi, A., Liotta, D., Ruggieri, G., Capezzuoli, E., Meccheri, M., Dini, A., 2016a. An overview on the characteristics of geothermal carbonate reservoirs in southern Tuscany. Ital. J. Geosci. 135, 17-29. https://doi.org/10.3301/IJG.2014.41

Brogi, A., Alçiçek, M.C., Yalçıner, C.C., Capezzuoli, E., Liotta, D., Meccheri, M., Rimondi, V., Ruggieri, G., Gandin, A., Boschi, C., Büyüksaraç, A., Alçiçek, H., Bülbül, A., Baykara, M.O., Shen, C., 2016b. Hydrothermal fluids circulation and travertine deposition in an active tectonic setting: Insights from the Kamara geothermal area (western Anatolia, Turkey). Tectonophysics, 680, 211-232. https://doi.org/10.1016/j.tecto.2016.05.003

Brogi, A., Capezzuoli, E., Kele, S., Baykara, M.O., Shen, C.-C., 2017. Key travertine tectofacies for neotectonics and palaeoseismicity reconstruction: effects of hydrothermal overpressured fluid injection. J. Geol. Soc. London 174, 676–699. https://doi.org/10.1144/jgs2016-124

Brogi, A., Liotta, D., Capezzuoli, E., Matera, P.F., Kele, S., Soligo, M., Tuccimei, P., Ruggieri, G., Yu, T.-L., Shen, C.-C., Huntington, K., 2020. Travertine deposits constraining transfer zone neotectonic activity in geothermal areas: an example from the inner Northern Apennines (Bagno Vignoni-Val d'Orcia area, Italy). Geothermics, 85, 101763. https://doi.org/10.1016/j.geothermics.2019.101763

Bülbül, A., 2000. Kamara ve Çizmeli (Yenice-Buldan) Sıcak ve Mineralli Sularının Hidrojeolojisi. PAÜ Fen Bilimleri Enstitüsü, Denizli, Turkey (MSc. Thesis, (in Turkish)).

Bülbül, A., Tarcan, G., Gökgöz, A., 2005. Denizli ili kuzeyinde yer alan bazı termal kaynakların hidrojeokimyasal incelenmesi ve kullanım özellikleri. 1. Tıbbi Jeoloji Sempozyumu Kitabı, Ankara, Turkey, pp. 251–255.

Caine, S.J., Evans, J.P., Forster, C.B., 1996. Fault zone architecture and permeability structure. Geology 24:1025–1028. doi:10.1130/00917613(1996)024\1025:FZAAPS[2.3.CO;2

Caine, J.S. Forster, C.B., 1999. Fault Zone Architecture and Fluid Flow: Insights from Field Data and Numerical Modeling. Geophys. Monog. Series. 113:101-127. https://doi.org/10.1029/GM113p0101

Çakır, Z., 1999. Along-strike discontinuity of active normal faults and its influence on Quaternary travertine deposition: examples from Western Turkey. Turk. J. Earth Sci. 8, 67–80.

Camanni, G., Roche, V., Childs, C., Manzocchi, T., Walsh, J.J., Coneally, J., Saqab, M.M., Delogkos, S., 2019. The three-dimensional geometry of relay zones within segmented normal faults. J. Struct. Geol. https://doi.org/10.1016/j.jsg.2019.103895

Capezzuoli, E., Gandin, A., Pedley, H.M., 2014. Decoding tufa and travertine (freshwater carbonates) in the sedimentary record: the state of the art. Sedimentology 61, 1–21. https://doi.org/10.1111/sed.12075

Capezzuoli, E., Ruggieri, G., Rimondi, V., Brogi, A., Liotta, D., Alçiçek, M.C., Alçiçek, H., Bülbül, A., Gandin, A., Meccheri, M., Shen, C.C., Bayakara, M.O., 2018. Calcite veining and feeding conduits in a hydrothemal system: Insights from a natural section across the Pleistocene Gölemezli travertine depositional system (western Antolia, Turkey). Sediment. Geol. 364, 180-203. https://doi.org/10.1016/j.sedgeo.2017.12.012

Cartwright, J.A., Mansfield, C.S., Trudgill, B., 1996. The growth of faults by segment linkage. Geological Society London Special Publications 99(1), 163-177. https://doi.org/10.1144/GSL.SP.1996.099.01.13

Childs, C., Watterson, J., Walsh, J.J., 1995. Fault overlap zones within developing normal fault systems. J. Geol. Soc. London 152, 535–549. London. https://doi.org/10.1144/gsjgs.152.3.0535

Childs, C., Worthington, R.P., Walsh, J.J., Roche, V., 2019. Conjugate relay zones: geometry of displacement transfer between opposed-dipping normal faults. J. Struct. Geol. 118, 377-390. https://doi.org/10.1016/j.jsg.2018.11.007

Collins, A.S., Robertson, A.H.F., 1997. Lycian melange, southwestern Turkey: an emplaced Late Cretaceous accretionary complex. Geology 25, 255–8. https://doi.org/10.1130/0091-7613(1997)025<0255:LMSTAE>2.3.CO;2

Coolbaugh, M.F., Raines, G.L., Zehner, R.E., Shevenell, L.A., Williams, C.F., 2006b. Prediction and discovery of new geothermal resources in the Great Basin: Multiple evidence of a large undiscovered resource base. Geoth. Res. T. 30, 867-873.

Cox, S.F., 1999. Deformational controls on the dynalics of fluid flow in mesothermal gold systems. Geological Society London Special Publications, 5, 123-140.

Cox, S.F., Knackstedt, M.A., Braun, J., 2001. Principles of Structural Control on Permeability and Fluid Flow in Hydrothermal Systems (Structural Controls on Ore Genesis). Society of Economic Geologists 24. pp. 1–24 Chapter 1. DOI:10.5382/rev.14.01

Crider, J.G., Pollard, D.D., 1998. Fault linkage: Three‐dimensional mechanical interaction between echelon normal faults. J. Geophys. Res. 103, 24,373-24,391. https://doi.org/10.1029/98JB01353

Curewitz, D., Karson, J.A., 1997. Structural settings of hydrothermal outflow: fracture permeability maintained by fault propagation and interaction. J. Volcanol. Geoth. Res. 79, 149–168. doi: 10.1016/S0377-0273(97)00027-9. https://doi.org/10.1016/S0377-0273(97)00027-9

De Filippis, L., Faccenna, C., Billi, A., Anzalone, E., Brilli, M., Özkul, M., Soligo, M., Tuccimei, P., Villa, I., 2012. Growth of fissure ridge travertines from geothermal springs of Denizli basin, western Turkey. Geol. Soc. Am. Bull. 124, 1629–1645. https://doi.org/10.1130/B30606.1

Evans, J.P., Forster, C.B., Goddard, J.V., 1997. Permeability of fault related rocks, and implications for hydraulic structure of fault zones. J. Struct. Geol. 19, 1393–404. https://doi.org/10.1016/S0191-8141(97)00057-6

Faulds J.E., Hinz N.H. 2015. Favorable Tectonic and Structural Settings of Geothermal Systems in the Great Basin Region, Western USA: Proxies for Discovering Blind Geothermal Systems. Proceedings World Geothermal Congress 2015 Melbourne, Australia, 19-25 April 2015

Fyfe, W.S., 1978. The evolution of the Earth's crust: modern plate tectonics to ancient spot tectonics? Chem. Geol. 23, 89-114. https://doi.org/10.1016/0009-2541(78)90068-2

Ford, T.D. Pedley, H.M., 1996. A review of tufa and travertine deposits of the world. Earth Sci. Rev. 41:117–175. https://doi.org/10.1016/S0012-8252(96)00030-X

Fossen, H., Rotevatn, A., 2016. Fault linkage and relay structures in extensional settings - A review. Earth Sci. Rev. 156, 14-28. https://doi.org/10.1016/j.earscirev.2015.11.014

Fouke, B.W., Farmer, J.D., Des Marais, D.J., Pratt L., Sturchio, N.C., Burns, P.C., Discipulo, M.K., 2000. Depositional facies and aqueous-solid geochemistry of travertine depositing hot springs (Angel Terrace, Mammoth Hot Springs, Yellowstone National Park, U.S.A.). J. Sediment. Res. 70, 565–585. DOI: 10.1306/2dc40929-0e47-11d7-8643000102c1865d

Gündoğan, İ., Helvacı, C., Sözbilir, H., 2008. Gypsiferous carbonates at Honaz Dağı (Denizli): first documentation of Triassic gypsum in western Turkey and its tectonic significance. J. Asian Earth Sci. 32, 49–65. https://doi.org/10.1016/j.jseaes.2007.09.005

Hancock, P.L., Chalmers, R.M.L., Altunel, E., Çakır, Z., 1999. Travitonics: using travertines in active fault studies. J. Struct. Geol. 21, 903–916. https://doi.org/10.1016/S0191-8141(99)00061-9

Irmak, T.S., 2013. Focal mechanism of small-moderate earthquakes in Denizli graben (SW Turkey). Earth Planets Space 65, 943–955. doi:10.5047/eps.2013.05.011

James, E.F., Hinz, N.H., Coolbaugh, M.F., Cashman, P.H., Kratt, C., Dering G., Edwards, J., Mayhew, B., McLachlan., H., 2011. Assessment of Favorable Structural Settings of Geothermal Systems in the Great Basin, Western USA. In: Transactions. GRC Anual Meeting; 2011/10/23; San Diego, CA. Davis, CA: Geothermal Resources Council; p. 777–783

Jourde, H., Flodin, E.A., Aydın, A., Durlofsky, L.J., Wen, X., H., 2002. Computing permeability of fault zones in Eolian sandstone from outcrop measurements. Am. Assoc. Pet. Hydrol. Bull., 86(7), 1187– 1200.

Kaymakçı, N., 2006. Kinematic development and paleostress analysis of the Denizli Basin (Western Turkey): implications of spatial varition of relative paleostress magnitudes and orientations. J. Asian Earth Sci. 27, 207–222. https://doi.org/10.1016/j.jseaes.2005.03.003

Kim, Y.-S., Peacock, D.C.P., Sanderson, D.J., 2003. Strike-slip faults and damage zones at Marsalforn, Gozo Island, Malta. Journal of Structural Geology, 25, 793-812. https://doi.org/10.1016/S0191-8141(02)00200-6

Kim, Y.-S., Peacock, D.C.P., Sanderson, D.J., 2004. Fault damage zones. J. Struct. Geol. 26, 503-517. https://doi.org/10.1016/j.jsg.2003.08.002

Koçyiğit, A., 2005. The Denizli graben–horst system and the eastern limit of western Anatolian continental extension: basin-fill, structure, deformational mode, throw amount and episodic evolutionary history, SW Turkey. Geodin. Acta 18, 167–208. https://doi.org/10.3166/ga.18.167-208

Konak, N., Şenel, M., 2002. Geological Map of Turkey in 1/500.000 Scale: Denizli Sheet. Publication of Mineral Research and Exploration Directorate of Turkey (MTA), Ankara.

Larsen, P.-H., 1988. Relay structures in a Lower Permian basementinvolved extension system, East Greenland. J. Struct. Geol. 10, 3-8. https://doi.org/10.1016/0191-8141(88)90122-8

Lebatard, A.-E., Alçiçek, M.C., Rochette, P., Khatib, S., Vialet, A., Boulbes, N., Bourlès, D.L., Demory, F., Guipert, G., Mayda, S., Titov, V.V., Vidal, L., de Lumley, H., 2014. Dating the Homo erectus bearing travertine from Kocabaş (Denizli, Turkey) at at least 1.1 Ma. Earth Planet. Sc. Lett. 390, 8–18. https://doi.org/10.1016/j.epsl.2013.12.031

Liotta, D., Ruggieri, G., Brogi, A., Fulignati, P., Dini, A., Nardini, I., 2010. Migration of geothermal fluids in extensional terrains: the ore deposits of the Boccheggiano-Montieri area (southern Tuscany, Italy). Int. J. Earth. Sci. 99, 623–644. DOI 10.1007/s00531-008-0411-3

Liotta, D., Brogi, A., Ruggieri, G., Rimondi, V., Zucchi, M., Helgadóttir, H.M., Montegrossi, G., Friðleifsson, G.Ó., 2020. Fracture analysis, hydrothermal mineralization and fluid pathways in the Neogene Geitafell central volcano: Insights for the Krafla active geothermal system. J. Volcanol. Geoth. Res. 391, 106502. https://doi.org/10.1016/j.jvolgeores.2018.11.023

Mancini, A., Frondini, F., Capezzuoli, E., Galvez Mejia, E., Lezzi, G., Matarazzi, D., Brogi, A., Swennen, R., 2019. Evaluating the geogenic CO2 flux from geothermal areas by analysing Quaternary travertine masses. New data from western Central Italy and review of previous CO2 flux data, Quat. Sci. Rev. 215, 132-143. https://doi.org/10.1016/j.quascirev.2019.04.030

Martinez-Diaz, J., Hernández-Enrile, J.L., 2001. Using travertine deformations to characterize paleoseismic activity along an active oblique-slip fault: The Alhama de Murcia fault (Betic Cordillera, Spain). Acta Geologica Hispanica 36(3), 3-4, 296-313.

Mayolle, S., Soliva, R., Caniven, Y., Wibberley, C.A.J., Ballas, G., Milesi, G., Dominguez, S., 2019. Scaling of fault damage zones in carbonate rocks. J. Struct. Geol. 124, 35-50. DOI: https://doi.org/10.1016/j.jsg.2019.03.007

Mesci, B.L., Gürsoy, H., Tatar, O., 2008. The evolution of travertine masses in the Sivas Area (Central Turkey) and their relationships to active tectonics. Turk. J. Earth Sci. 17, 219–240.

Muir-Wood, R., 1993. Neohydrotectonics. Zeitschrift für Geomorphologie. Supplement 94, 275–284.

Nishikawa, O., Furuhashi, K., Masuyama, M., Ogata, T., Shiraishi, T., Shen, C.-C., 2012. Radiocarbon dating of residual organic matter in travertine formed along the Yumoto Fault in Oga Peninsula, northeast Japan:

Implications for long-term hot spring activity under the influence of earthquakes. Sediment. Geol. 243–244, 181–190 https://doi.org/10.1016/j.sedgeo.2011.11.001

Nixon, C.W., Vaagan, S., Sanderson, D.J., Gawthorpe, R.L., 2018. Spatial distribution of damage and strain within a normal fault relay at Kilve, U.K. J. Struct. Geol. 118, 194-209. https://doi.org/10.1016/j.jsg.2018.10.016

Olvera-García, E., Garduño-Monroy, V.H., Liotta, D., Brogi, A., Bermejo-Santoyo, G., Guevara-Alday, J.A. 2020. Neogene-Quaternary normal and transfer faults controlling deep-seated T geothermal systems: The case of San Agustín del Maíz (central Trans-Mexican Volcanic Belt, México). Geothermics 86, 101791. https://doi.org/10.1016/j.geothermics.2019.101791

Okay, A. İ., 1989. Denizli'nin güneyinde Menderes masifi ve Likya naplarının jeolojisi. Bull. Miner. Res. Expl. Direct. Turkey (MTA) 109, 45–58.

Özkul, M., Kele, S., Gökgöz, A., Shen, C., Jones, B., Baykara, M.O., F⊠rizs, I., Németh, T., Chang, Y., Alçiçek, M.C., 2013. Comparison of the Quaternary travertine sites in the Denizli extensional basin based on their depositional and geochemical data. Sediment. Geol. 294, 179 – 204. https://doi.org/10.1016/j.sedgeo.2013.05.018

Pamir, H.N., Erentöz, C., 1974. Geological Maps of Turkey in 1:500.000 Scale: Denizli Sheet. Publication of Mineral Research and Exploration Directorate of Turkey (MTA), Ankara, Turkey.

Peacock, D.C.P., Sanderson, D.J., 1991. Displacements, segment linkage and relay ramps in normal fault zones. J. Struct. Geol. 13 (6), 721–733. DOI: 10.1306/BDFF9046-1718-11D7-8645000102C1865D

Peacock, D.C.P., Sanderson, D.J., 1994. Geometry and development of relay ramps in normal fault systems. Bull. Am. Assoc. Pet. Geol. 78, 147–165.

Peacock, D.C., 2002. Propagation, interaction and linkage in normal fault systems. Earth Sci. Rev. 58(1-2), 121-142. https://doi.org/10.1016/S0012-8252(01)00085-X

Pentecost, A., 2005. Travertine, Springer, Berlin (445 pp.).

Piccardi, L., 2007. The AD 60 Denizli Basin earthquake and, G. the apparition of Archangel Michael at Colossae (Aegean Turkey). Myth and Geology, 273, Special Publication of the Geological Society, 95-105. https://doi.org/10.1144/GSL.SP.2007.273.01.08

Piper, J.D.A., Mesci, L., Gürsoy, H., Tatar, O., Davies, C., 2007. Palaeomagnetic and rock magnetic properties of travertine: Its potential as a recorder of geomagnetic palaeosecular variation, environmental change and earthquake activity in the Sıcak Çermik geothermal field, Turkey. Phys. Earth Planet. In. 161(1), 50-73. https://doi.org/10.1016/j.pepi.2007.01.006

Polak, A., Elsworth, D. Yasuhara, H., Grader, A.S., Halleck, P.M., 2003. Permeability reduction of a natural fracture under net dissolution by hydrothermal fluids. Geophys. Res. Lett. 30(20), 2020, https://doi.org/10.1029/2003GL017575

Ramsay, J.G., 1980. The crack-seal mechanism of rock deformation. Nature 284, 125–139. https://doi.org/10.1038/284135a0

Rowland, J.V., Sibson, R.H., 2004. Structural controls on hydrothermal flowing a segmented rift system, Taupo Volcanic Zone, New Zealand. Geofluids 4, 259–28. https://doi.org/10.1111/j.1468-8123.2004.00091.x

Ruhl, C.J., Abrecrombie, R.E., Smith, K.D., Zaliapin, I., 2016. Complex spatiotemporal evolution of the 2008 Mw 4.9 Mogur earthquake swarm (Reno, Nevada): interplay of fluid and faulting. J. Geophys. Res-Sol. Ea. 121(11), 8196-8216. https://doi.org/10.1002/2017JB014850

Şaroğlu, F., Emre, Ö., Boray, A., 1987. Türkiye'nin Diri fayları ve depremselliği. General Directorate of Mineral Research and Exploration of Turkey (MTA), Ankara, Scientific Report No: 8174.

Şaroğlu, F., Emre, Ö., Kuşçu, İ., 1992. Active faultmap of Turkey, Scale 1:1.000.000. General Directorate of Mineral Research and Exploration of Turkey, Ankara.

Sengör, A.M.C., Yılmaz, Y., 1981. Tethyan evolution of Turkey, a plate tectonic approach. Tectonophysics 75, 181–241. https://doi.org/10.1016/0040-1951(81)90275-4

Shelly,, D.R., Taira, T., Prejean, S.G., Hill, D.P., Dreger, D.S. 2015. Fluid-faulting interactions: fracture-mesh and fault-valve behavior in the Febrauary 2014 Mammoth Mountain, California, earthquake swarm. Geophys. Res. Lett. 42, 5803-5812. https://doi.org/10.1002/2015GL064325

Sibson, R.H., 1977. Fault rocks and fault mechanisms. J. Geol. Soc. London 133, 191-213. https://doi.org/10.1144/gsjgs.133.3.0191

Sibson, R.H., 1981. Fluid flow accompanying faulting: field evidence and models. In: Earthquake Predicion (Eds: D.S. Simpson and P.G. Richards). AGU Washington, D.C. https://doi.org/10.1029/ME004p0593

Sibson, R.H., 1987. Earthquake rupturing as a mineralising agent in hydrothermal systems. Geology 15, 701–708. https://doi.org/10.1130/0091-7613(1987)15<701:ERAAMA>2.0.CO;2

Sibson, R.H., 1996. Structural permeability of fluid-driven fault–fracture meshes. J. Struct. Geol. 18, 1031–1042.

Sibson, R.H., 2000. Fluid involvement in normal faulting. J. Geody. 29, 469–499. https://doi.org/10.1016/S0264-3707(99)00042-3

Şimşek, Ş., 1984. Denizli, Kızıldere-Tekkehamam-Tosunlar-Buldan-Yenice alanının jeolojisi ve jeotermal enerji olanakları. Mineral Research and Exploration Directorate of Turkey (MTA), Scientific Report No: 7846, Ankara, Turkey (in Turkish).

Şimşek, Ş., Günay, G., Elhatip, H., Ekmekçi, M., 2000. Environmental protection of geothermal waters and travertines at Pamukkale, Turkey. Geothermics 22, 557-572. https://doi.org/10.1016/S0375-6505(00)00022-5

Sun, S., 1990. Denizli-Uşak Arasının Jeolojisi ve Linyit Olanakları. Mineral Research and Exploration Directorate of Turkey (MTA), Scientific Report, 9985, Ankara, Turkey (in Turkish).

Temiz, U., Eikenberg, J. 2011. U/Th dating of the travertine deposited at transfer zone between two normal faults and their neotectonic significance: Cambazlı fissure ridge travertines (the Gediz graben-Turkey). Geodin. Acta 24, 95–105. DOI: 10.3166/ga.24.95-105

ten Veen, J.H., Boulton, S.J., Alçiçek, M.C., 2009. From palaeotectonics to neotectonics in the Neotethys realm: the importance of kinematic decoupling and inherited structural grain in SW Anatolia (Turkey). Tectonophysics 473, 261–281. https://doi.org/10.1016/j.tecto.2008.09.030

Utku, M., 2009. Analysis of Denizli earthquakes according to their activity and cumulative activity terms. Mineral Res. Exp. Bull. 138, 7–33.

Uysal, I.T., Feng, Y., Zhao, J.X., Altunel, E., Weatherley, D., Karabacak, V., Cengiz, O., Golding, S.D., Lawrence, M.G., Collerson, K., D., 2007. U-series dating and geochemical tracing of late Quaternary travertine in co-seismic fissures. Earth Planet. Sci. Lett. 257 (3–4), 450–462. https://doi.org/10.1016/j.epsl.2007.03.004

Uysal, I.T., Feng, Y., Zhao, J.X., Isik, V., Nuriel, P., Golding, S.D., 2009. Hydrothermal CO2 degassing in seismically active zones during the late Quaternary. Chem. Geol. 265, 442–454. https://doi.org/10.1016/j.chemgeo.2009.05.011

van Hinsbergen, D.J.J., 2010. A key extensional metamorphic complex reviewed and restored: the Menderes Massif of western Turkey. Earth Sci. Rev. 102, 60–76. https://doi.org/10.1016/j.earscirev.2010.05.005

van Hinsbergen, D.J.J., Schmid, S.M., 2012. Map view restoration of Aegean–West Anatolian accretion and extension since the Eocene. Tectonics 31, TC5005. https://doi.org/10.1029/2012TC003132

Van Noten, K., Claes, H., Soete, J., Foubert, A., Özkul, M., Swennen, R., 2013. Fracture network and strike-slip deformation along reactivated normal faults in Quaternary travertine deposits, Denizli Basin, Western Turkey. Tectonophysics 588, 154–170. https://doi.org/10.1016/j.tecto.2012.12.018

Zucchi, M., Brogi, A., Liotta, D., Rimondi, V., Ruggieri, V., Montegrossi, G., Caggianelli, A., Dini, A., 2017. Permeability and hydraulic conductivity of faulted micaschist in the eastern Elba Island exhumed geothermal system (Tyrrhenian sea, Italy): insights from Cala Stagnone. Geothermics 70, 125-145. https://doi.org/10.1016/j.geothermics.2017.05.007

Zucchi, M., 2020. Faults controlling geothermal fluid flow in low permeability rock volumes: An example from the exhumed geothermal system of eastern Elba Island (northern Tyrrhenian Sea, Italy). Geothermics 85, 101765. https://doi.org/10.1016/j.geothermics.2019.101765

Figure Captions

Fig. 1 - Geological sketch-map of the Denizli Basin (modified after Sun, 1990 and Alçiçek et al., 2007) and location of the study area.

Fig. 2 - Geological map of the north-eastern margin of the Denizli Basin, where the Honalilar area (study area) is indicated.

Fig. 3 - a) Panoramic view of the Honalirar quarry with the main faults highlighted; b) Google Earth photograph showing the Honalilar quarry and the surroundings hills; the location of the scan lines measured and described in the text and illustrated in the Figure 12 is also indicated.

Fig. 4 - Panoramic view of the fault zone to the south of the quarry juxtaposing the Neogene sediments to the metamorphic units, where the hydrothermal altered footwall damage zone is highlighted.

Fig. 5 - a) The fault scarp in the southern prolongation of the eastern fault delimiting the step-over zone (see the text for more explanation). Panoramic view of the fault zone; c-d) particular of the damage volumes related to the fault zone.

Fig. 6 - Tectonic sketch-map of the study area showing the main structures associated with the step over zone. Main faults, travertine deposits, banded Ca-carbonate veins and the station of the structural analyses are also indicated. b) ~~G~~eological map of the same area.

Fig. 7 - Cartoon showing the main structures, the banded Ca-carbonate veins and the stereographic diagrams (lower hemisphere, ~~equiareal~~ projections) indicating fault and striae for each station of structural analysis.

Fig. 8 - Fault plane solutions diagrams with fault-trends and striae, reconstructed from the inversion of kinematic data collected on fault-slip surfaces and divided per structural domains of the step-over zone.

Fig. 9 - a) The faults delimiting the step-over zone have ~~an~~ oblique-slip left-lateral ~~kinematics~~ (average pitch 75°), implying a ratio = 0.26 between the horizontal and vertical offset. b) Fault plane solution for the average strike, ~~deep~~ and pitch values calculated for the fault segments 1 and 3; furthermore, the angular relation between the average fault and the associated theoretical T-fracture (mode I fracture) is shown. c) Relationships between the main fault and vein ~~trends~~ in the study area coupled with the direction of the theoretical T-fractures as calculated in (b).

Fig. 10 - Photographs illustrating the travertine deposits at the top of the quarry area: a) bedded travertine forming the eastern flank of the travertine fissure ridge reported in the Fig. 6; b) ~~particular of the~~ contact of the travertine deposit on the pre-Neogene metamorphic substratum. The basal part of the succession is characterised by a breccia cemented by carbonate; c) detail of the banded calcite vein filling the internal part of the fissure ridge; d) detail of planar-to-wavy layers of lime mudstone; e) example of well-bedded, cm-thick layers of clotted/peloidal microbial mats.

Fig- 11 - Photographs illustrating the banded Ca-carbonate veins exposed in the quarry and developed within W-E fault zones of the step-over zone.

Fig. 12 - a) Scan lines measured in the quarry; their location is shown in the Fig. 3; b) diagram illustrating the vein width variation along the scan line: the maximum value of 6 m has been measured; c) diagram illustrating the number of veins each 10 m along the scan line; d) diagram illustrating the number of veins with the indicated width; e) Stereographic (lower hemisphere, Schmidt diagram) and rose diagrams of the measured veins along the scan line; f) Fault and striae of the faults affecting the banded Ca-carbonate veins; g) location of the single scan lines with respect to the vein exposed in the quarry.

Fig. 13 - a) Photograph illustrating the fabric of the banded Ca-carbonate veins, ~~often~~ characterised by centimeter-scale breccia fragments of the calcite veins; b) Detail of the sharp contact separating the banded vein and host (metamorphic) rocks; c) crosscutting relationships of different generation of banded Ca-carbonate veins.

Fig. 14 - a) Photograph showing a banded Ca-carbonate vein developed within a fault zone affecting micaschist in the footwall of the eastern fault delimiting the step-over zone; b) detail of a minor vein highlighting the symmetry of the bands; c-d) details of the hydrofractured metamorphic rocks nearby the fault zones.

Fig. 15 - a-b) Photograph illustrating cataclasites associated ~~to~~ W-E faults within the step over zone and cemented by yellowish carbonate; c) Photograph illustrating a cataclasite ~~level~~ formed at the contact with the banded Ca-carbonate vein.

Fig. 16 - a-b) Photographs of the kinematic indicators (calcite fiber steps) characterising slip surfaces affecting the banded Ca-carbonate veins; c) example of dm-scale shear band localised within a banded Ca-carbonate vein and developed parallel to the banding.

Fig. 17 - Diagram of the relationship between relay-width and relay-length in step-over zones; data from the study area is compared with a broad dataset reported in Fossen and Rotevatn (2016).

Fig. 18 – Conceptual geometrical model of the study area, where the main veins and faults developed within the step-over zone are considered structures formed within an highly dilatational volume.

Fig. 19 - Cartoon showing the orientation of the fissure ridge-type travertine deposits developing in a releasing step-over zone bridging faults characterised by a dominant normal kinematics with a slight oblique-slip component (in this case the ratio between horizontal and vertical components has been calculated at 0.26).

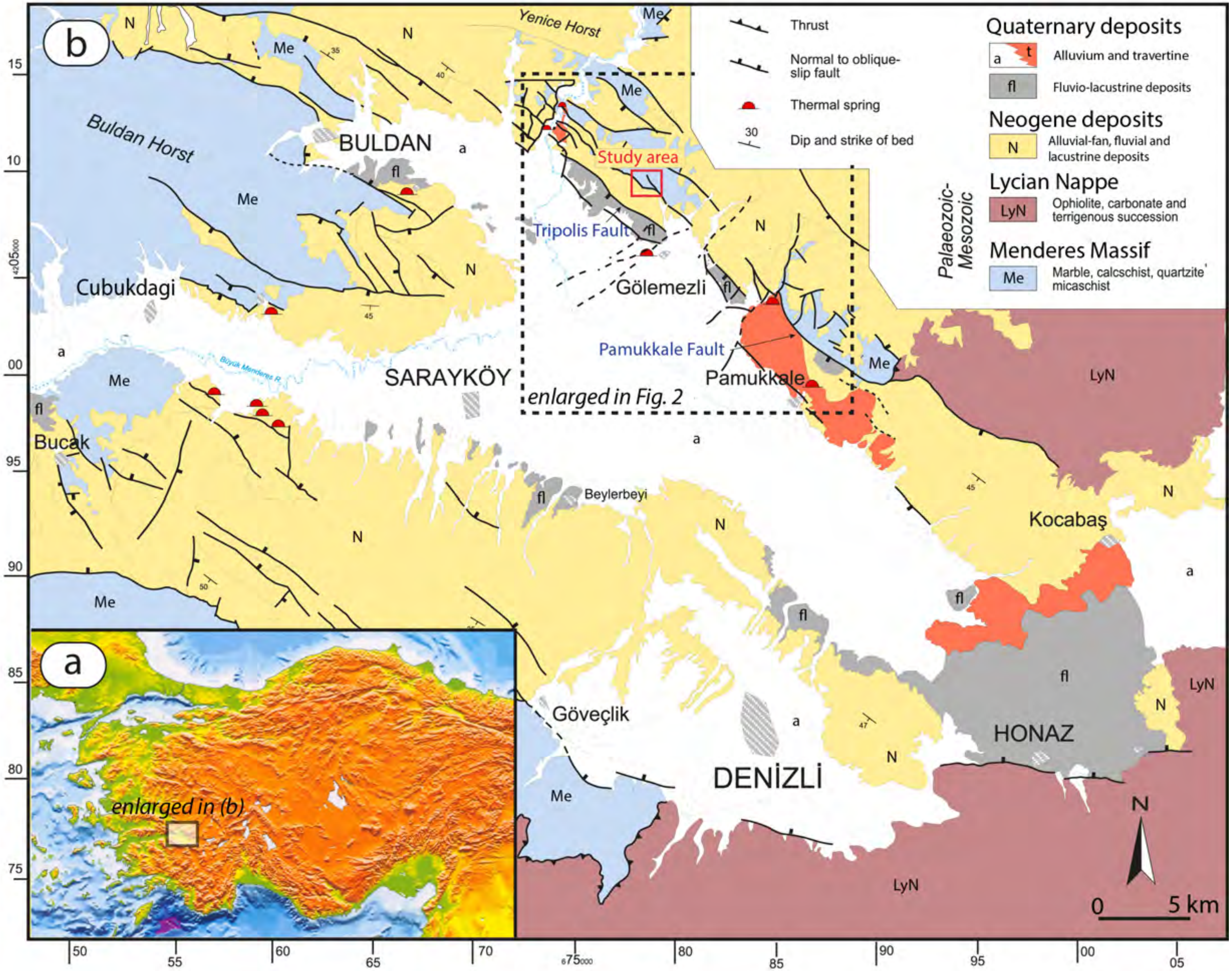

b
a
Thrust
Normal to oblique-slip fault
Thermal spring
Dip and strike of bed
Quaternary deposits
Alluvium and travertine
Fluvio-lacustrine deposits
Neogene deposits
Alluvial-fan, fluvial and lacustrine deposits
Lycian Nappe
Ophiolite, carbonate and terrigenous succession
Menderes Massif
Marble, calcschist, quartzite micaschist
Palaeozoic-Mesozoic
Yenice Horst
Buldan Horst
BULDAN
Study area
Tripolis Fault
Cubukdagi
Gölemezli
Pamukkale Fault
Pamukkale
SARAYKÖY
enlarged in Fig. 2
Bucak
Beylerbeyi
Kocabaş
HONAZ
Göveçlik
DENİZLİ
enlarged in (b)
0 5 km
N

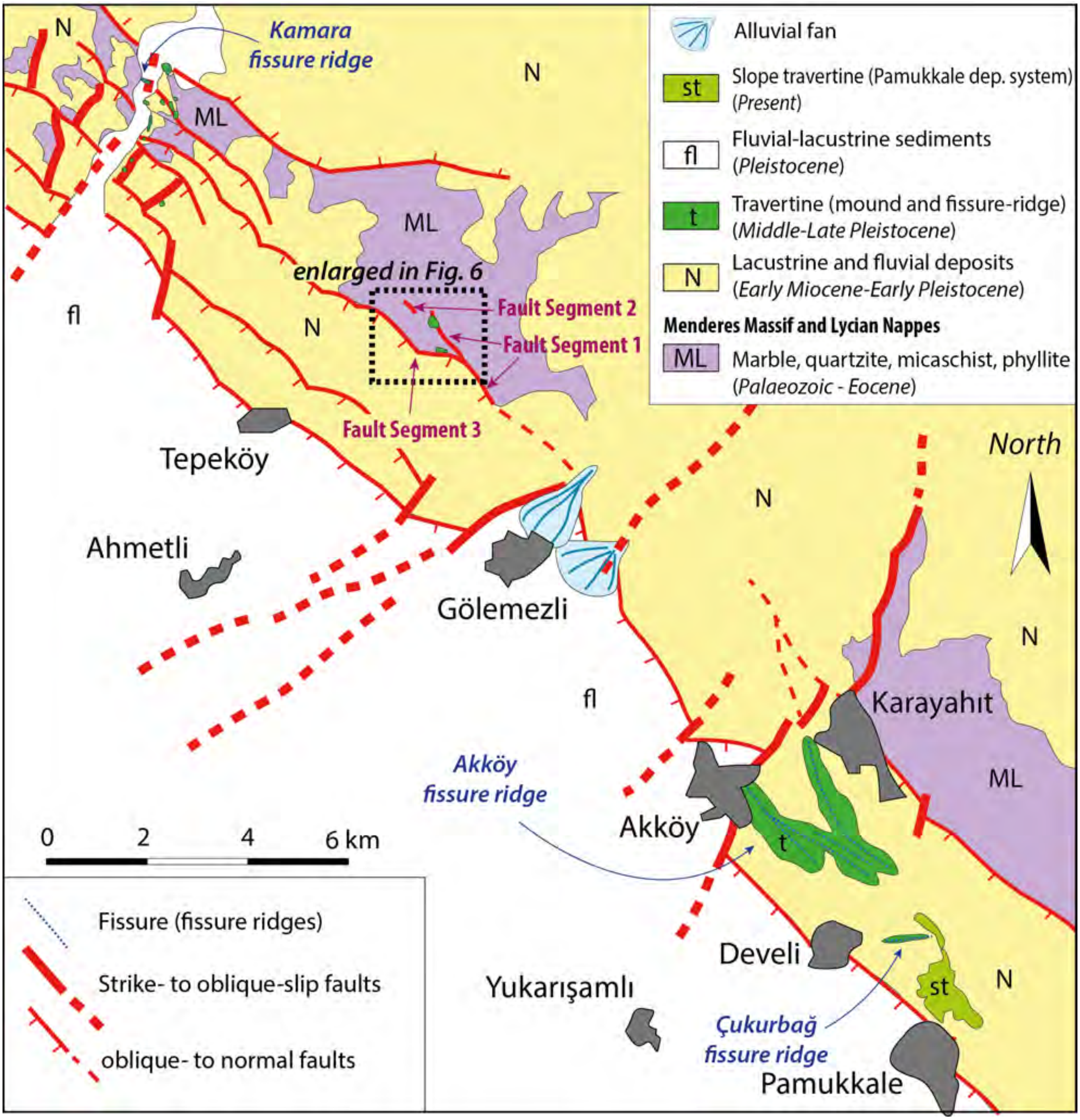

Kamara fissure ridge
N
ML
enlarged in Fig. 6
Fault Segment 2
Fault Segment 1
Fault Segment 3
fl
Tepeköy
Ahmetli
Gölemezli
Karayahıt
Akköy fissure ridge
Akköy
t
st
Develi
Yukarışamlı
Çukurbağ fissure ridge
Pamukkale
North
0 2 4 6 km
Alluvial fan
st Slope travertine (Pamukkale dep. system) (Present)
fl Fluvial-lacustrine sediments (Pleistocene)
t Travertine (mound and fissure-ridge) (Middle-Late Pleistocene)
N Lacustrine and fluvial deposits (Early Miocene-Early Pleistocene)
Menderes Massif and Lycian Nappes
ML Marble, quartzite, micaschist, phyllite (Palaeozoic - Eocene)
Fissure (fissure ridges)
Strike- to oblique-slip faults
oblique- to normal faults

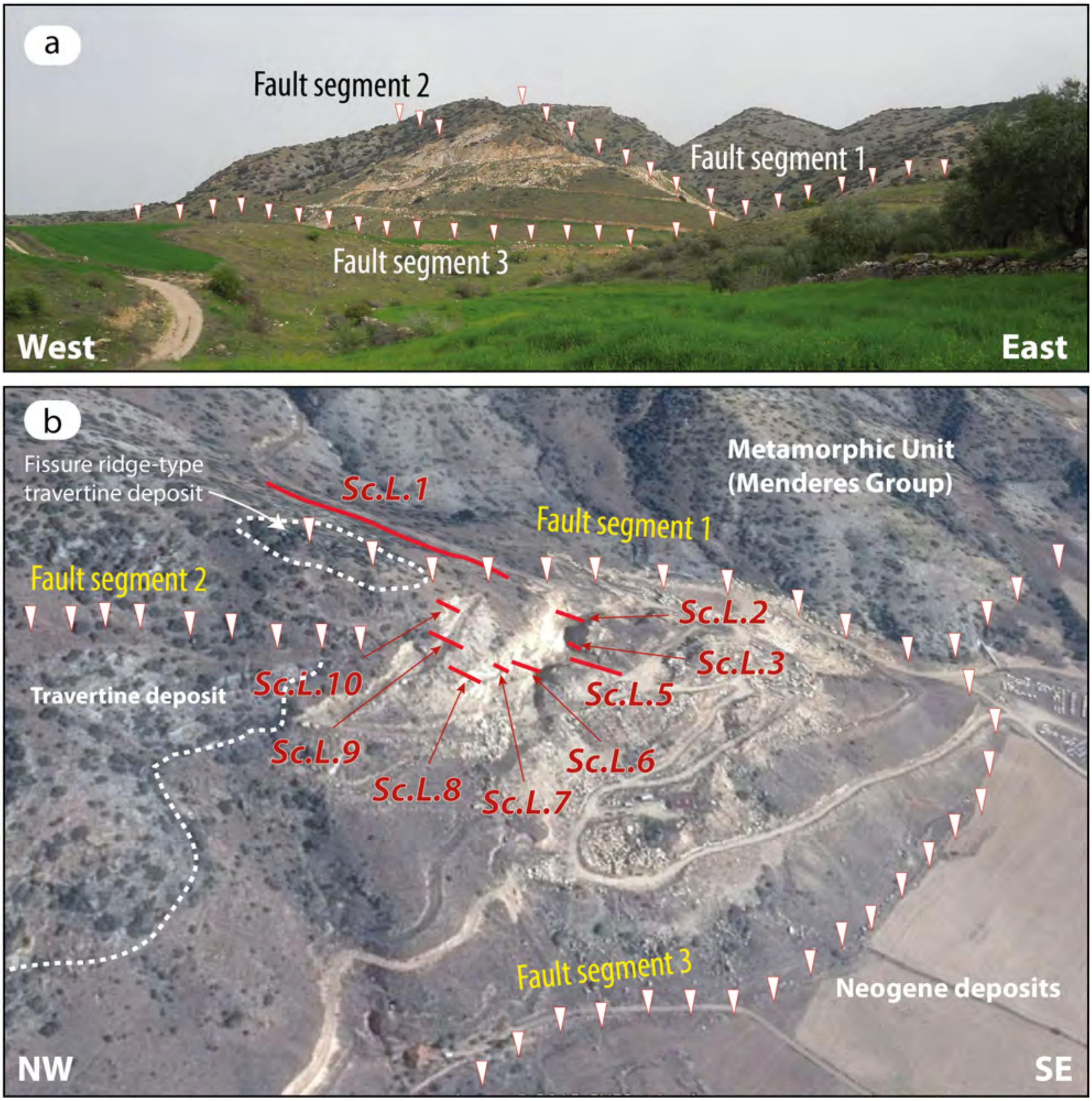
a
Fault segment 2
Fault segment 1
Fault segment 3
West
East
b
Fissure ridge-type
travertine deposit
Sc.L.1
Metamorphic Unit
(Menderes Group)
Fault segment 1
Fault segment 2
Sc.L.2
Sc.L.3
Sc.L.10
Travertine deposit
Sc.L.5
Sc.L.9
Sc.L.6
Sc.L.8
Sc.L.7
Fault segment 3
Neogene deposits
NW
SE

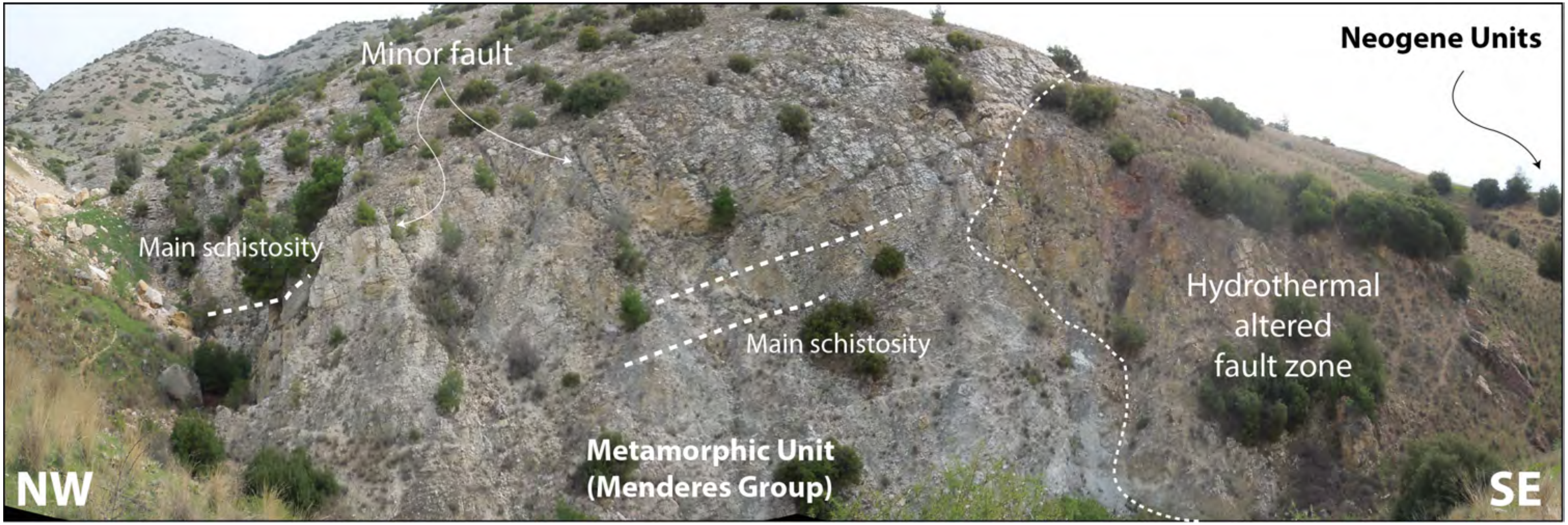

Minor fault
Neogene Units
Main schistosity
Main schistosity
Hydrothermal altered fault zone
Metamorphic Unit (Menderes Group)
NW
SE

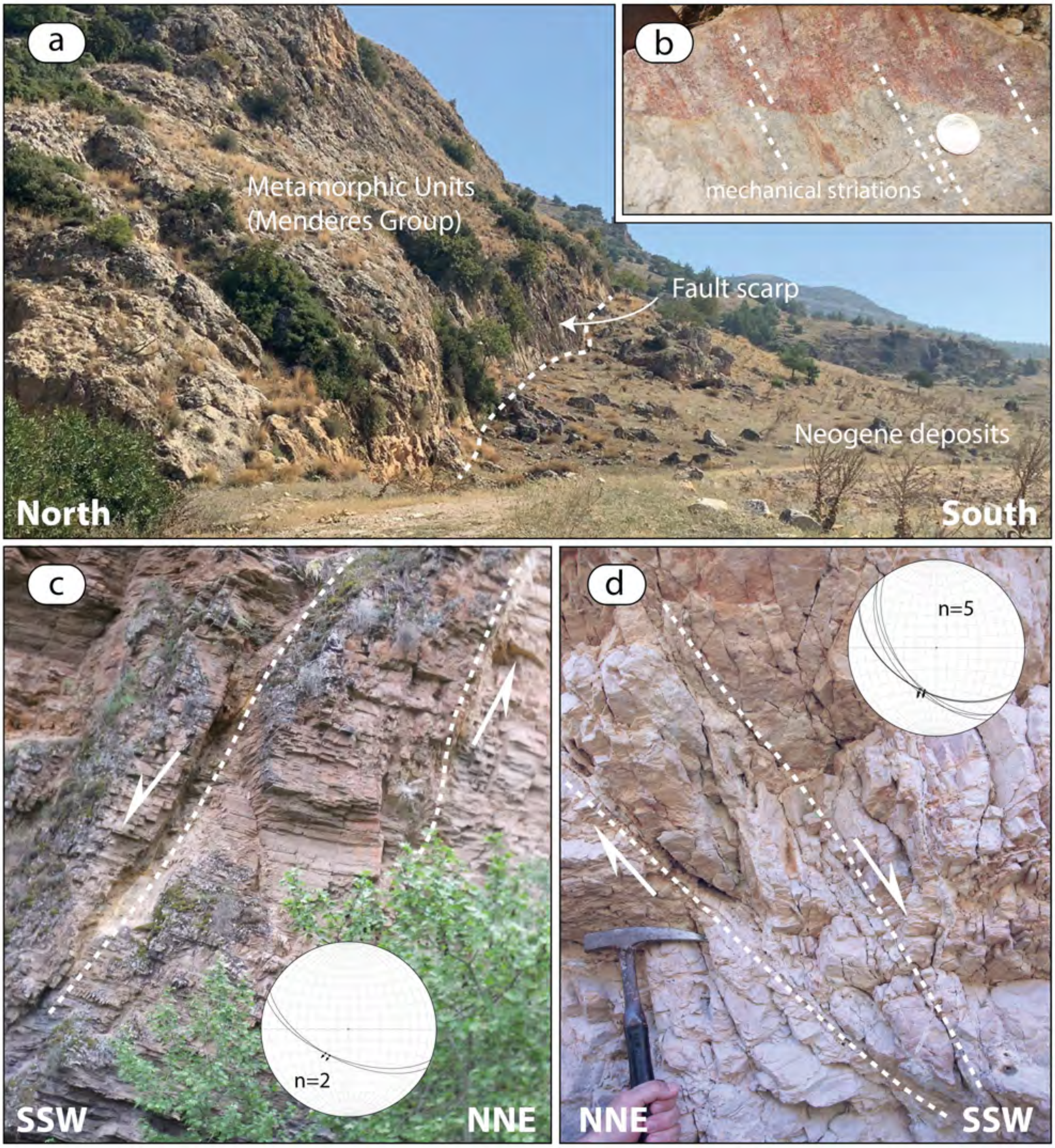
a
Metamorphic Units
(Menderes Group)
Fault scarp
Neogene deposits
North
South
b
mechanical striations
c
SSW
NNE
n=2
d
n=5
NNE
SSW

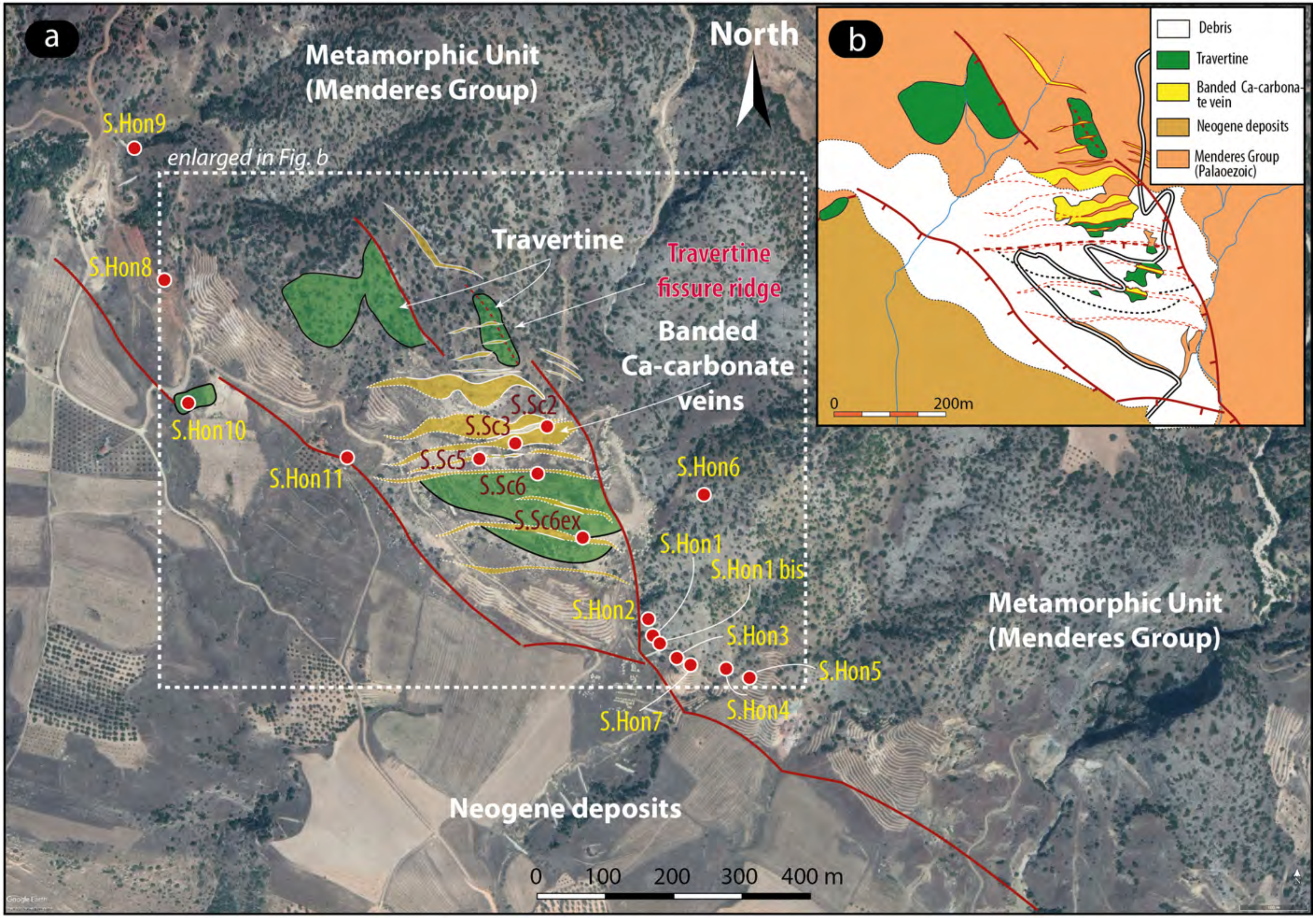
a
North
Metamorphic Unit
(Menderes Group)
S.Hon9
enlarged in Fig. b
Travertine
Travertine
fissure ridge
Banded
Ca-carbonate
veins
S.Hon8
S.Hon10
S.Hon11
S.Sc2
S.Sc3
S.Sc5
S.Sc6
S.Sc6ex
S.Hon6
S.Hon1
S.Hon1 bis
S.Hon2
S.Hon3
S.Hon5
S.Hon4
S.Hon7
Metamorphic Unit
(Menderes Group)
Neogene deposits
0 100 200 300 400 m
b
Debris
Travertine
Banded Ca-carbonate vein
Neogene deposits
Menderes Group
(Palaoezoic)
0
200m

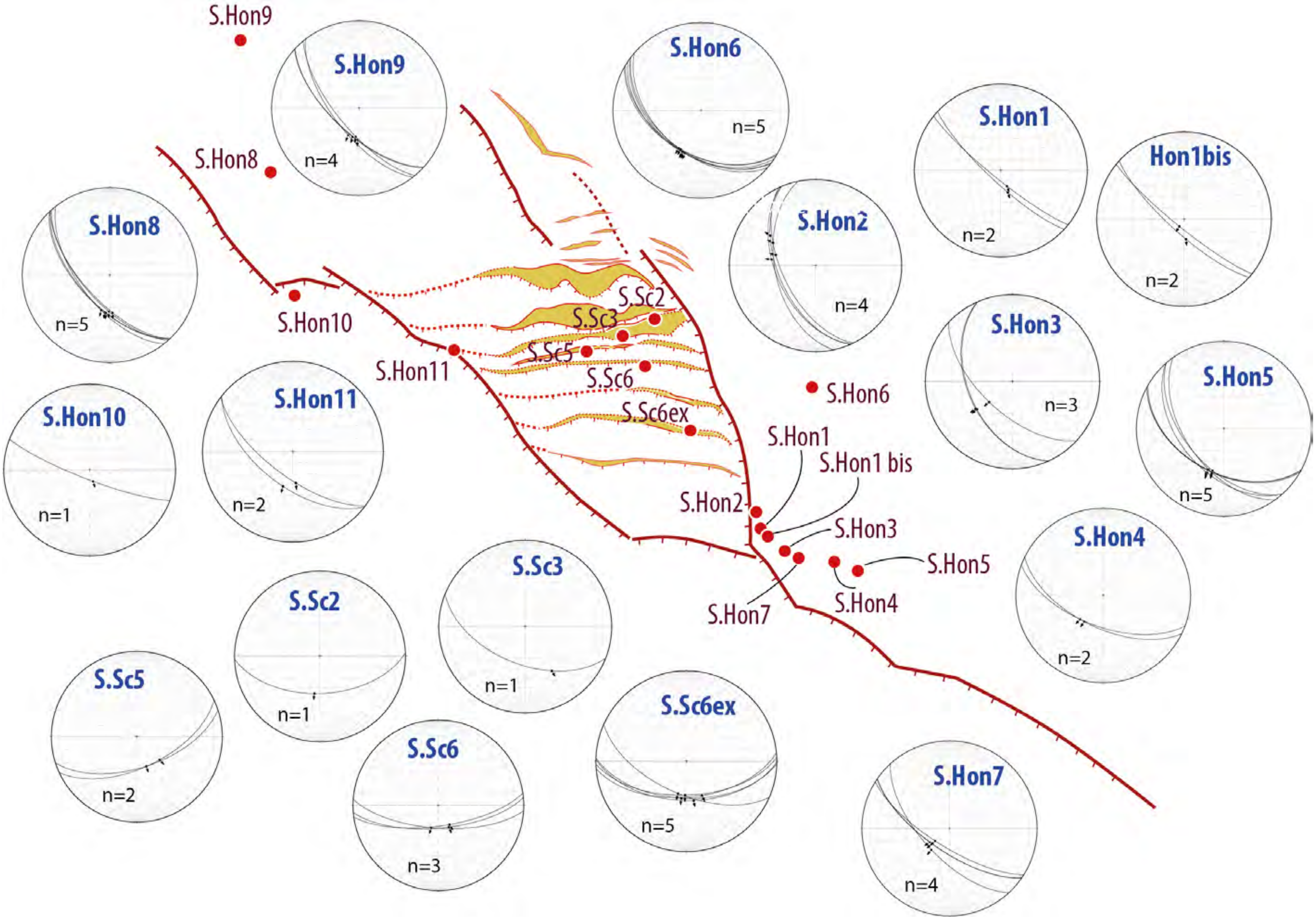

S.Hon9
S.Hon9
n=4
S.Hon6
n=5
S.Hon1
n=2
Hon1bis
n=2
S.Hon8
S.Hon8
n=5
S.Hon2
n=4
S.Hon10
S.Sc2
S.Sc3
S.Hon3
n=3
S.Sc5
S.Hon11
S.Sc6
S.Hon5
n=5
S.Hon6
S.Hon10
n=1
S.Hon11
n=2
S.Sc6ex
S.Hon1
S.Hon1 bis
S.Hon2
S.Hon3
S.Hon5
S.Hon4
S.Hon7
S.Hon4
n=2
S.Sc3
n=1
S.Sc2
n=1
S.Sc5
n=2
S.Sc6ex
n=5
S.Sc6
n=3
S.Hon7
n=4

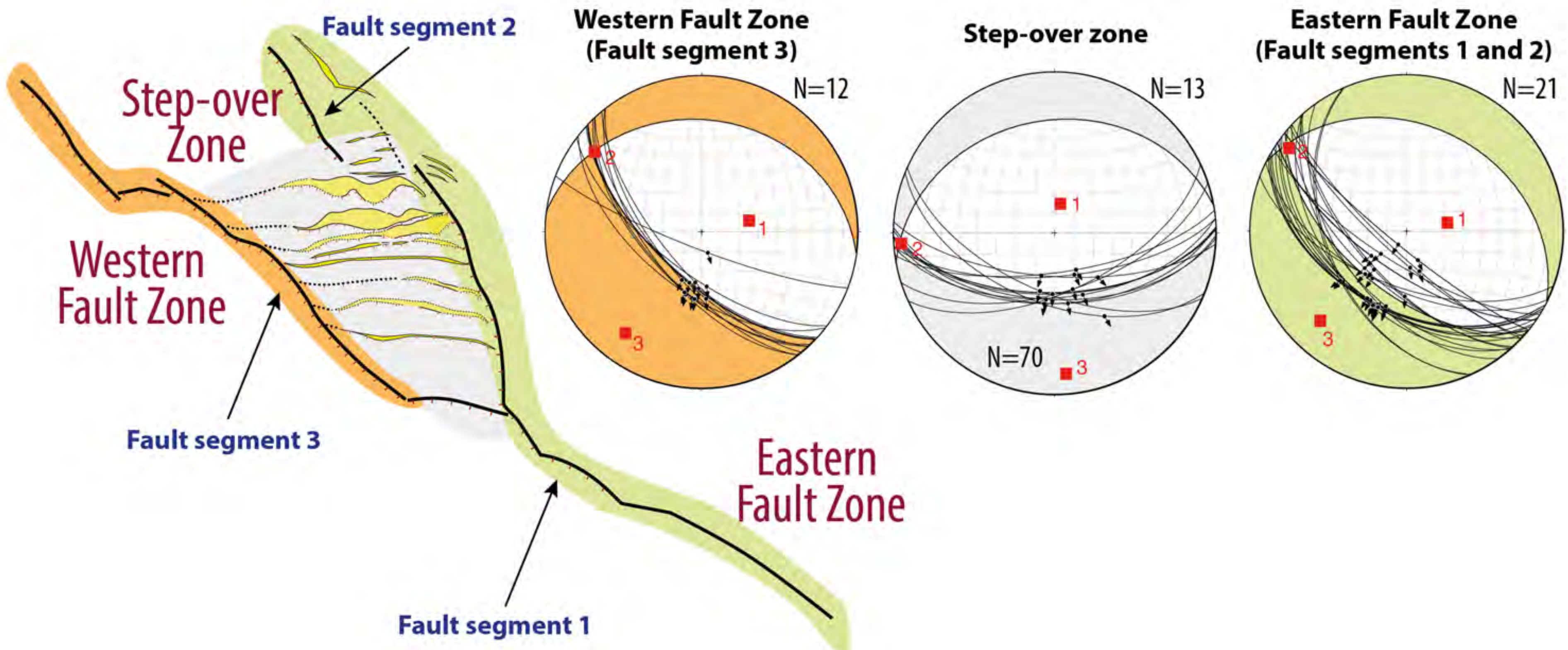
Fault segment 2
Step-over Zone
Western Fault Zone
Fault segment 3
Eastern Fault Zone
Fault segment 1
Western Fault Zone
(Fault segment 3)
N=12
Step-over zone
N=13
N=70
Eastern Fault Zone
(Fault segments 1 and 2)
N=21

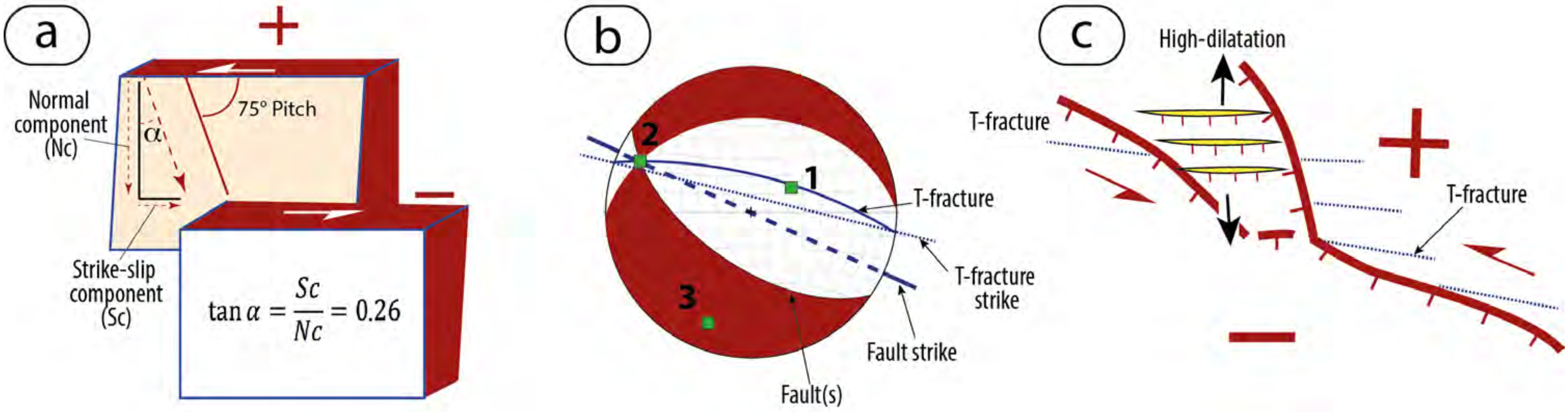
a
+
Normal component (Nc)
α
75° Pitch
Strike-slip component (Sc)
−
$\tan\alpha = \frac{Sc}{Nc} = 0.26$
b
2
1
3
T-fracture
T-fracture strike
Fault strike
Fault(s)
c
High-dilatation
T-fracture
+
T-fracture
−

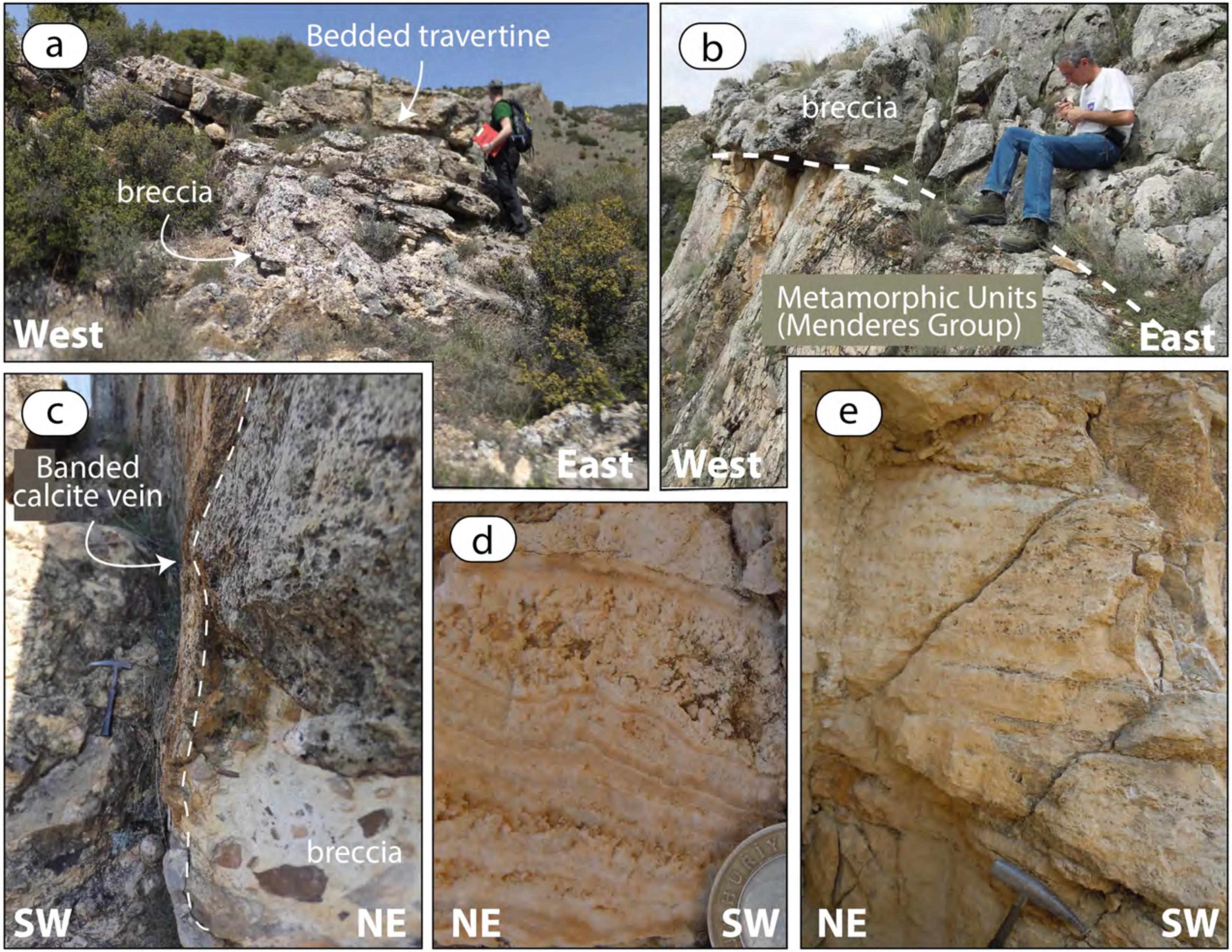
a
Bedded travertine
breccia
West
East
b
breccia
Metamorphic Units
(Menderes Group)
East
West
c
Banded
calcite vein
breccia
SW
NE
d
NE
SW
e
NE
SW

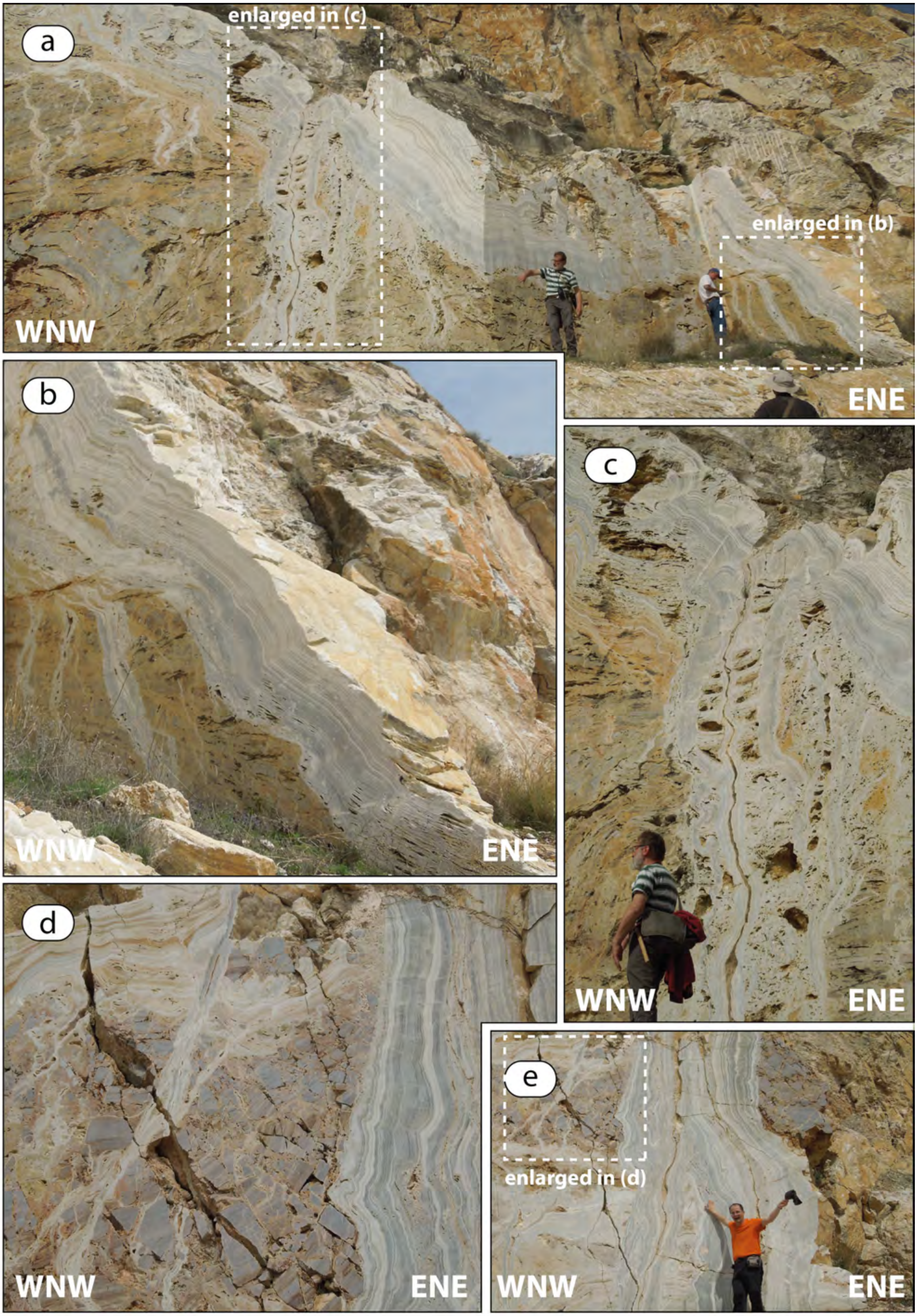

a
enlarged in (c)
enlarged in (b)
WNW
ENE
b
WNW
ENE
c
WNW
ENE
d
WNW
ENE
e
enlarged in (d)
WNW
ENE

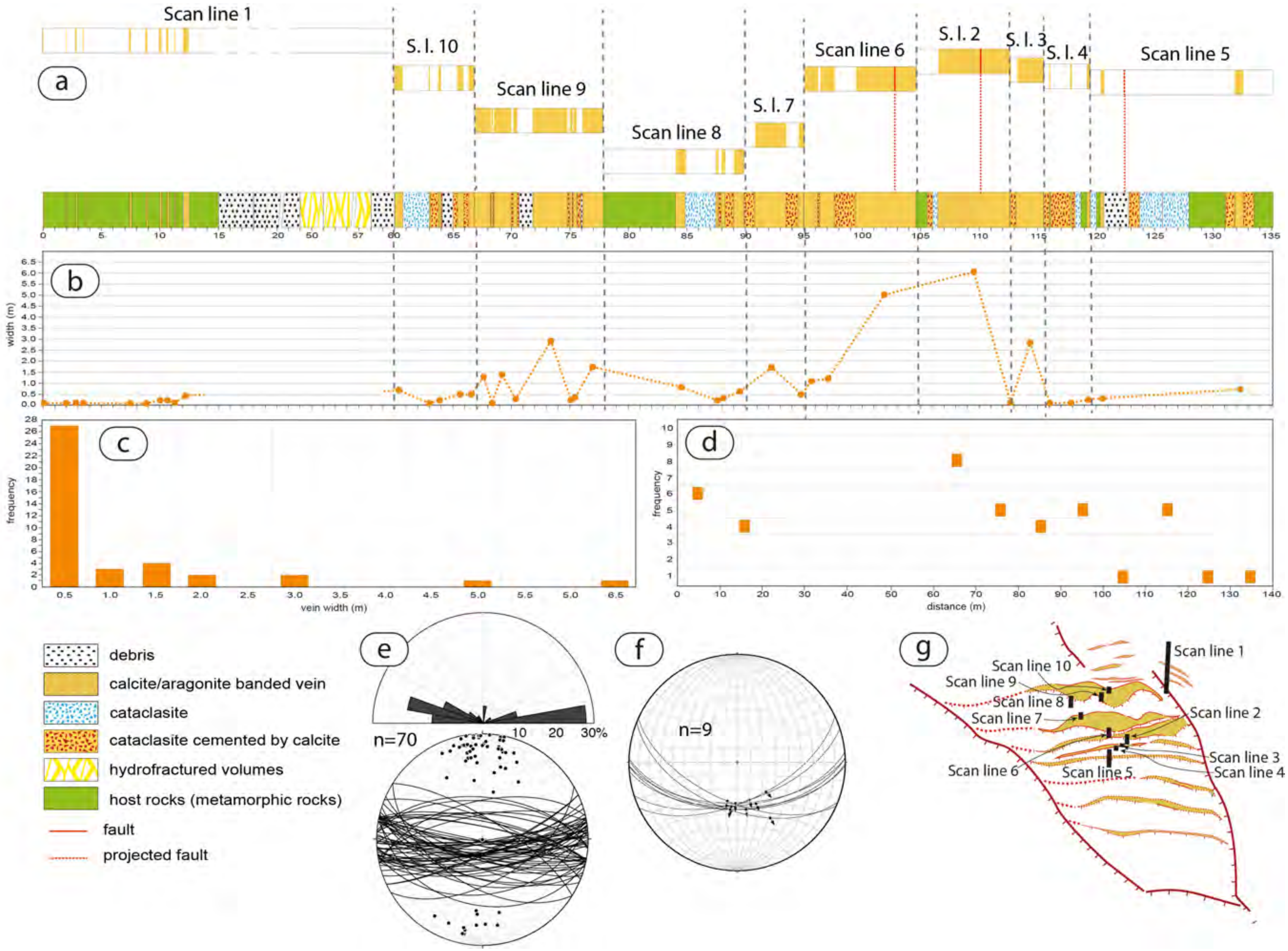

Scan line 1
S. l. 10
Scan line 9
Scan line 8
S. l. 7
Scan line 6
S. l. 2
S. l. 3
S. l. 4
Scan line 5
a
b
c
d
e
f
g
width (m)
frequency
vein width (m)
distance (m)
debris
calcite/aragonite banded vein
cataclasite
cataclasite cemented by calcite
hydrofractured volumes
host rocks (metamorphic rocks)
fault
projected fault
n=70
n=9
10
20
30%

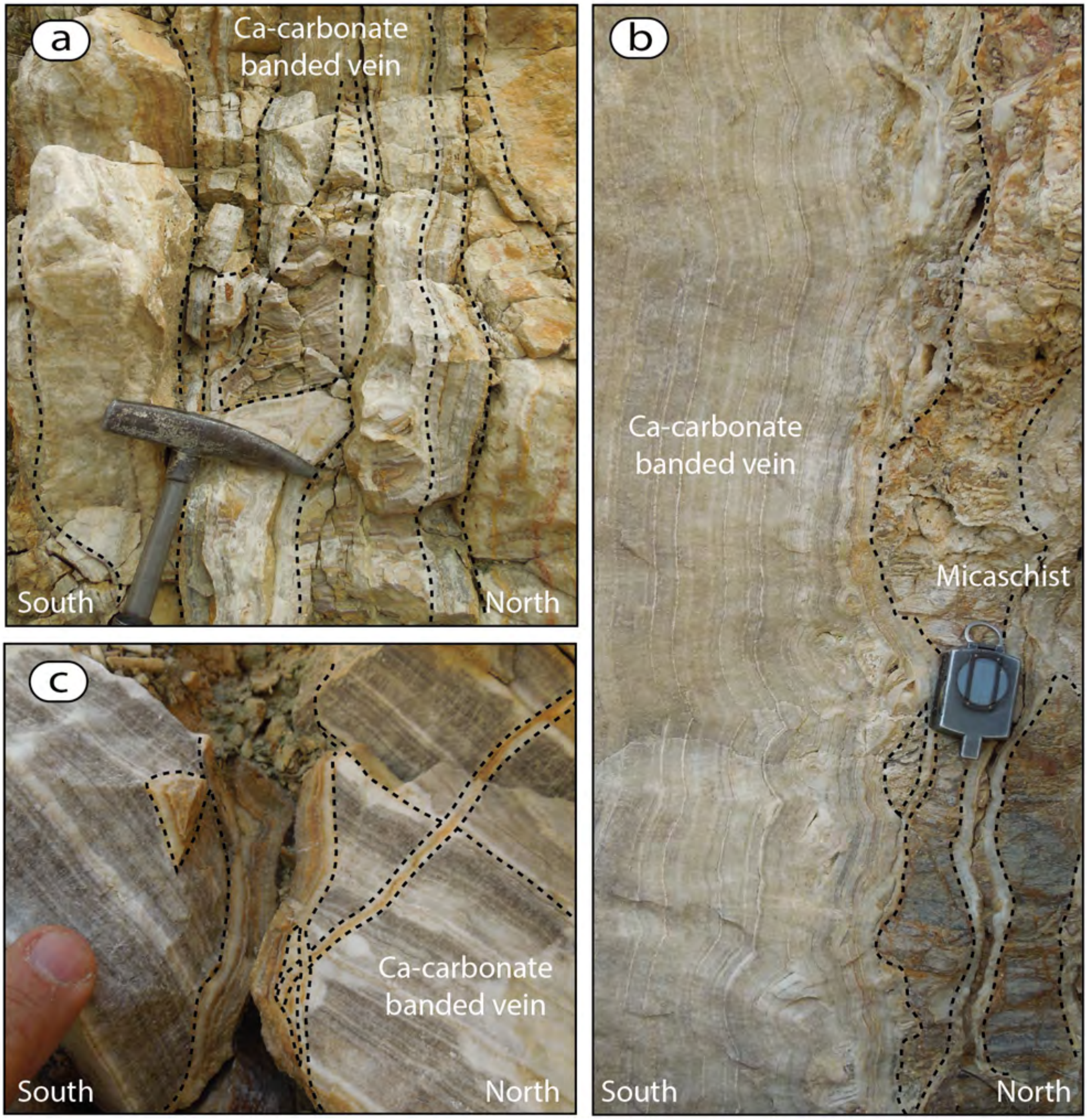
a
Ca-carbonate banded vein
South
North
b
Ca-carbonate banded vein
Micaschist
South
North
c
Ca-carbonate banded vein
South
North

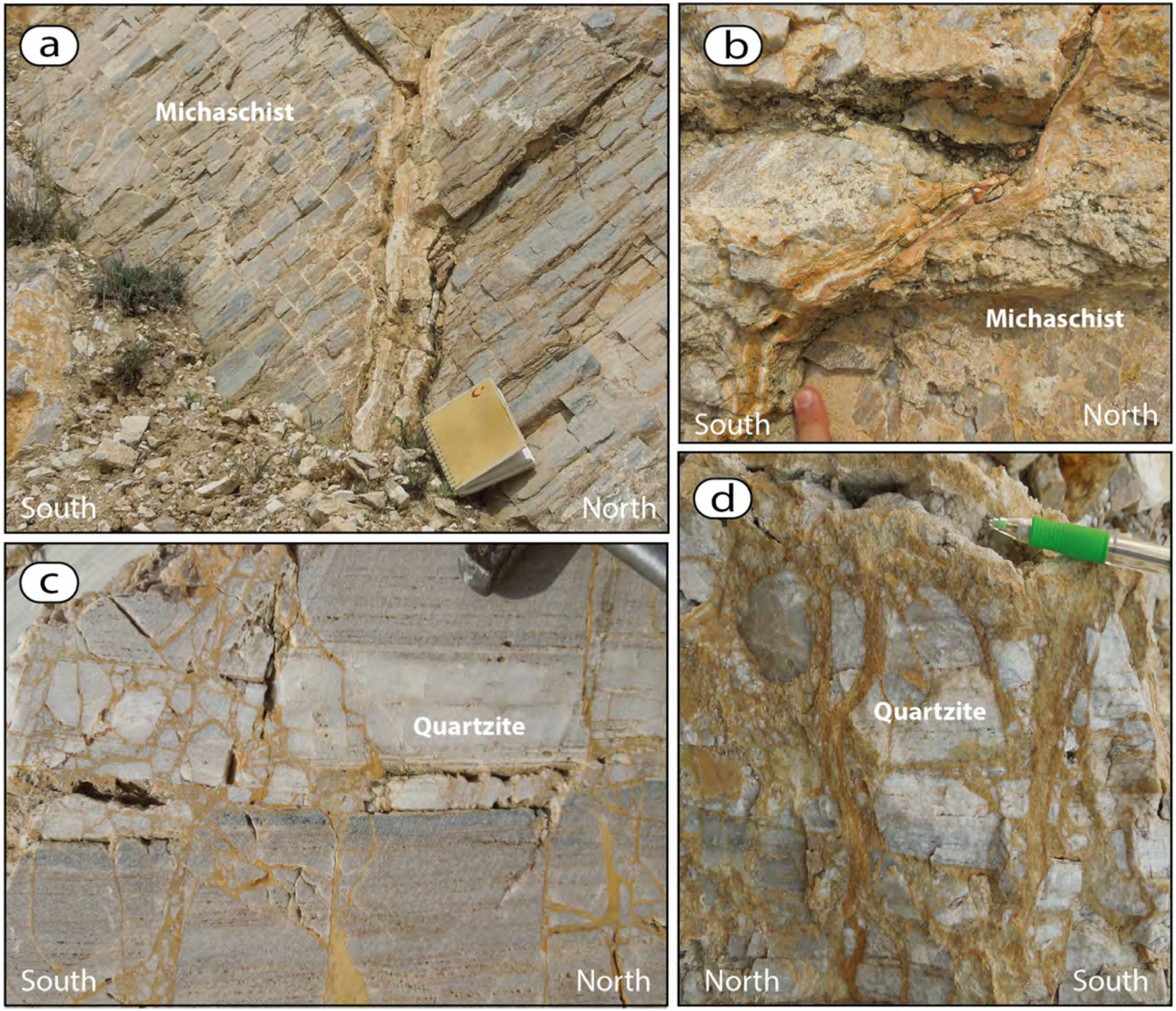
a
Michaschist
South
North
b
Michaschist
South
North
c
Quartzite
South
North
d
Quartzite
North
South

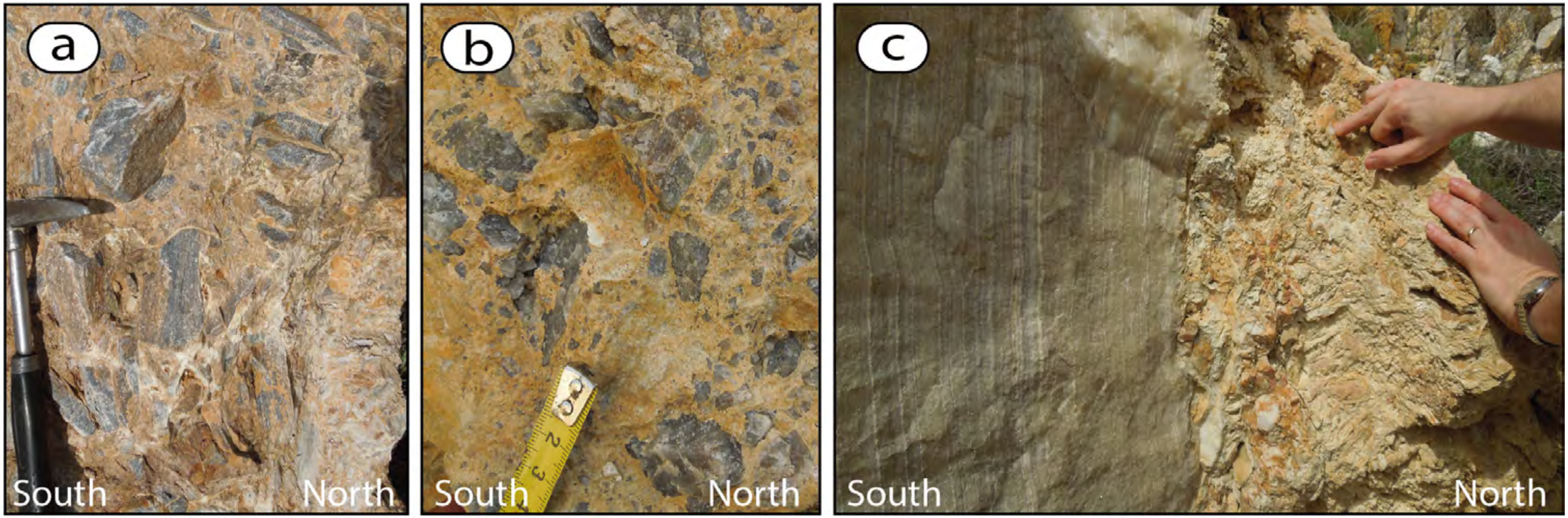
a
South
North
b
South
North
c
South
North

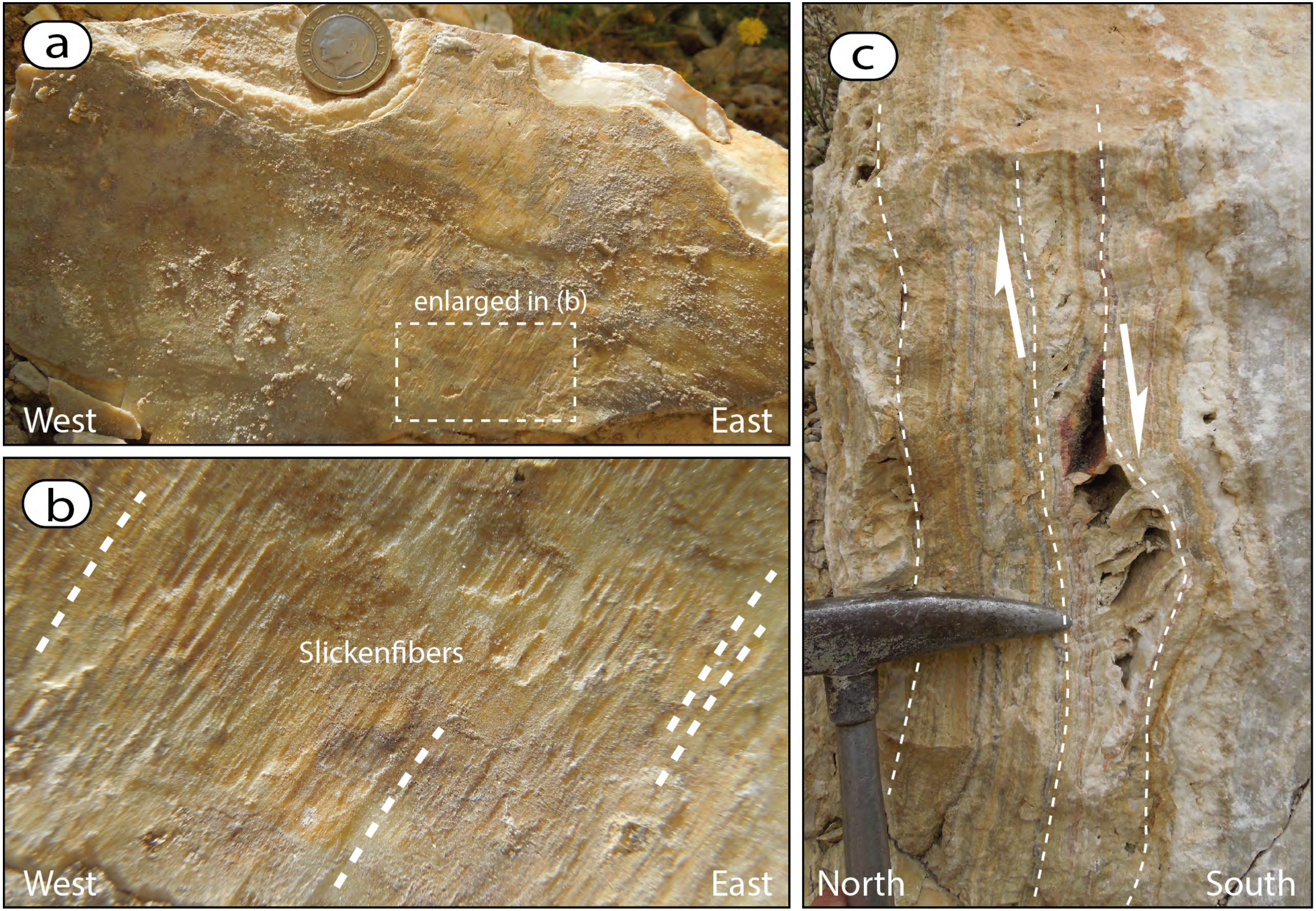
a
enlarged in (b)
West
East
b
Slickenfibers
West
East
c
North
South

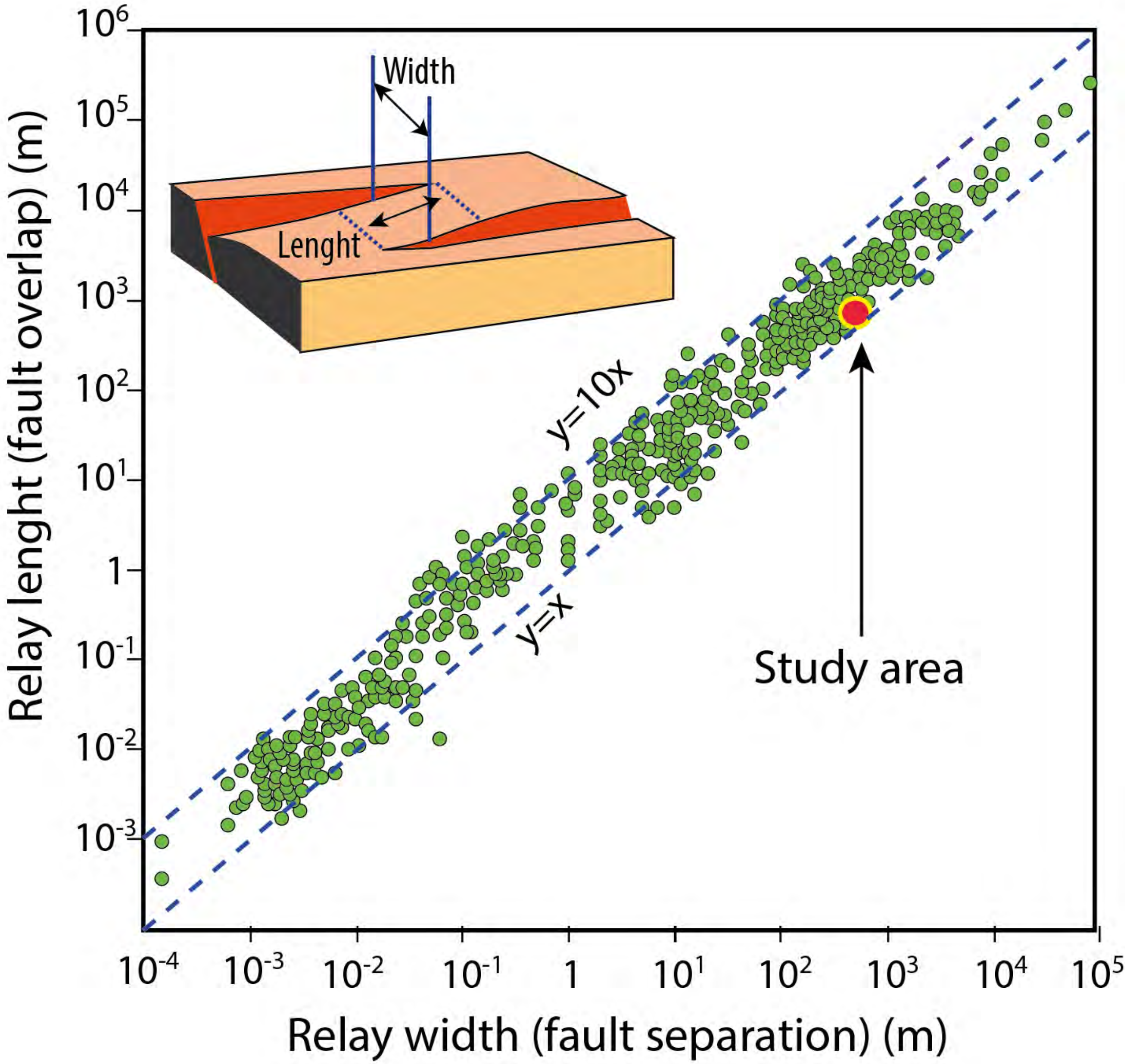

Width
Lenght
y=10x
y=x
Study area
Relay lenght (fault overlap) (m)
Relay width (fault separation) (m)
10^6
10^5
10^4
10^3
10^2
10^1
1
10^-1
10^-2
10^-3
10^-4
10^-3
10^-2
10^-1
1
10^1
10^2
10^3
10^4
10^5

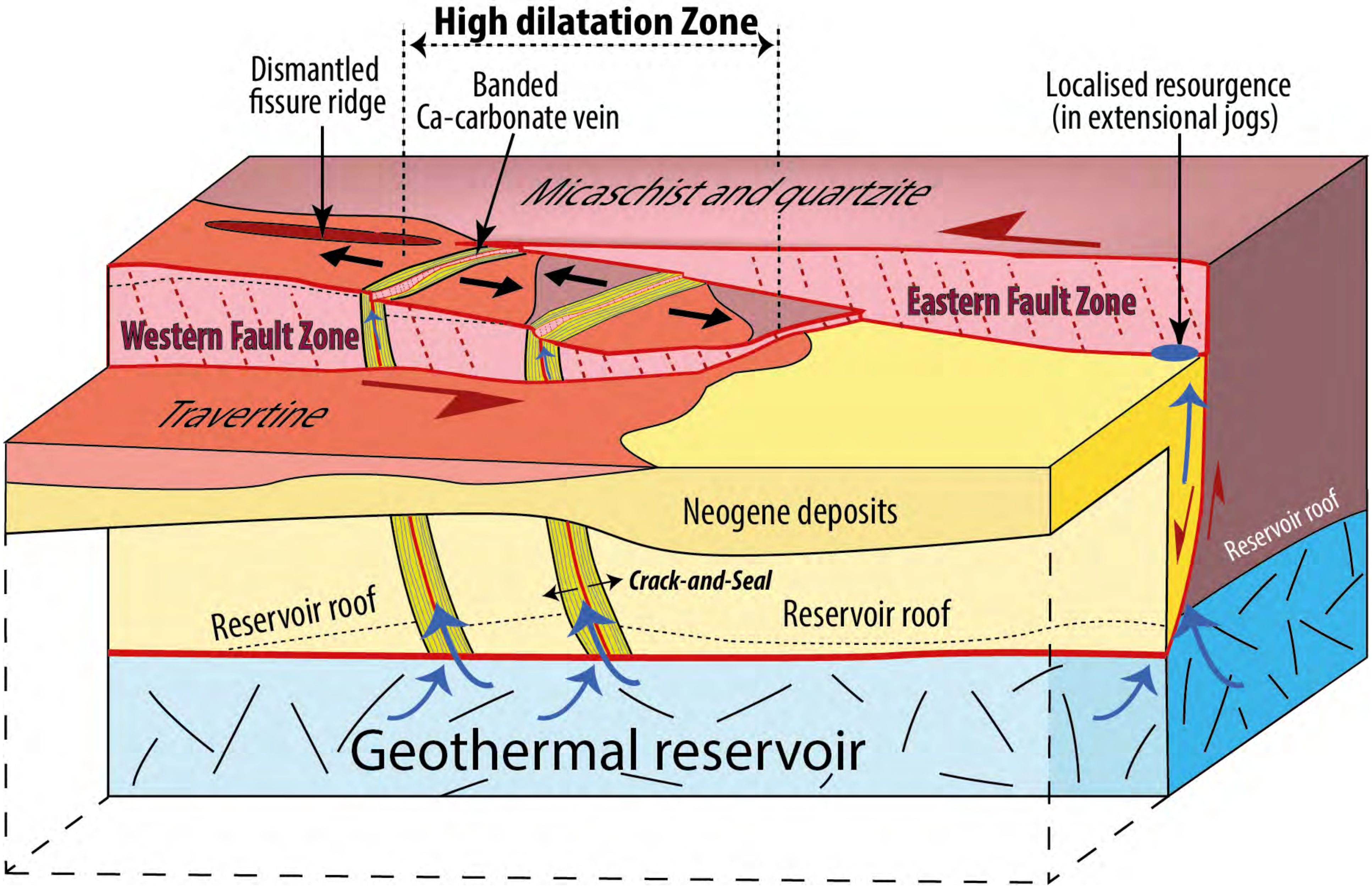
High dilatation Zone
Dismantled fissure ridge
Banded Ca-carbonate vein
Localised resourgence (in extensional jogs)
Micaschist and quartzite
Eastern Fault Zone
Western Fault Zone
Travertine
Neogene deposits
Crack-and-Seal
Reservoir roof
Reservoir roof
Reservoir roof
Geothermal reservoir

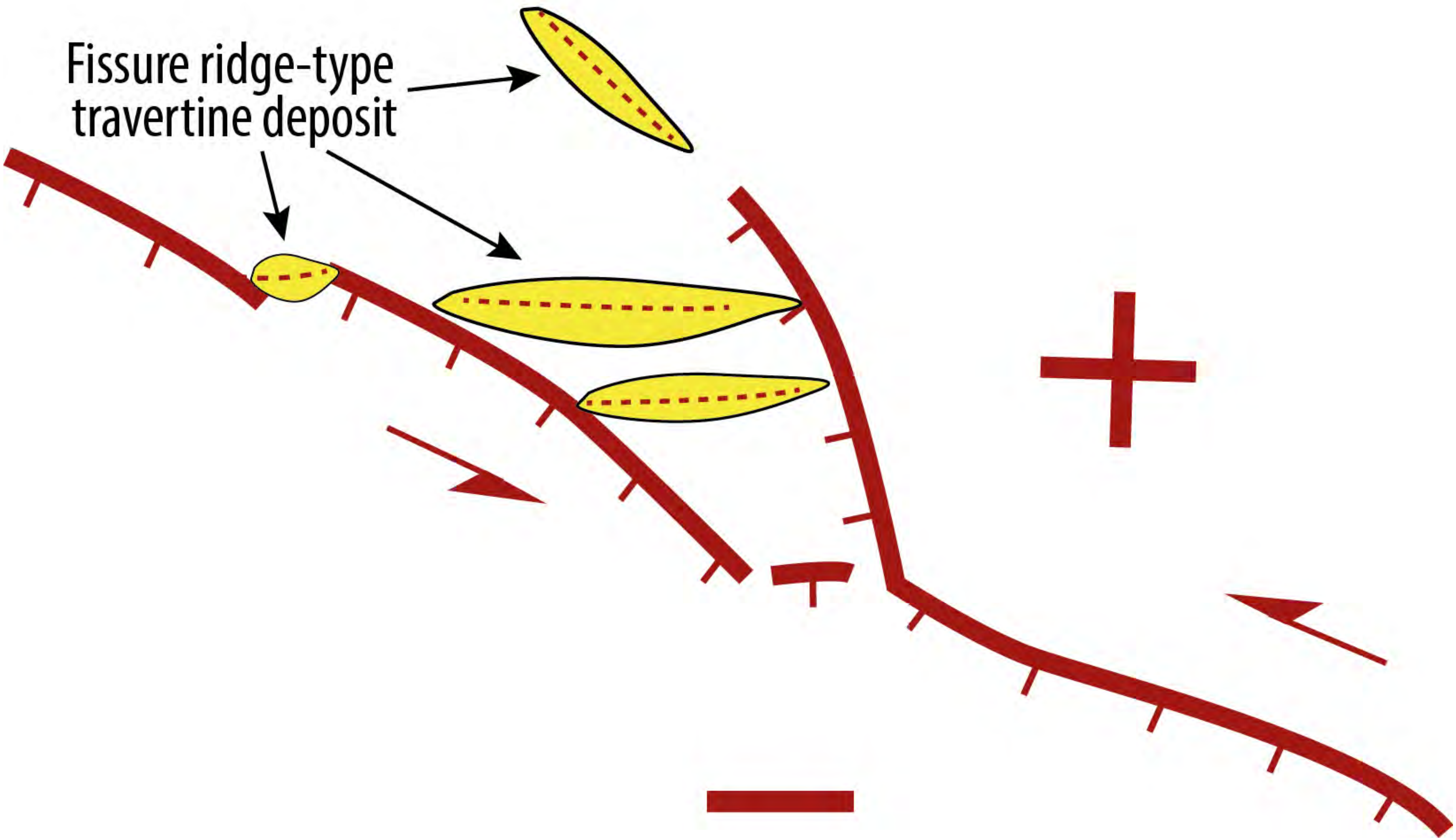
Fissure ridge-type
travertine deposit
+
−